Journal of Econometrics 222 (2021) 364–392

Contents lists available at ScienceDirect

Journal of Econometrics

journal homepage: www.elsevier.com/locate/jeconom

Closed-form implied volatility surfaces for stochastic volatility models with jumps☆

Yacine Aït-Sahalia [a,1], Chenxu Li [b,*], Chen Xu Li [c,2]

[a] Department of Economics, Princeton University and NBER, United States of America
[b] Guanghua School of Management, Peking University, PR China
[c] School of Business, Renmin University of China, PR China

ARTICLE INFO

Article history:
Available online 1 August 2020

JEL classification:
G12
C51
C52

Keywords:
Implied volatility surface
Stochastic volatility
Jumps
Option pricing
Closed-form expansion
Model selection

ABSTRACT

We develop a closed-form bivariate expansion of the shape characteristics of the implied volatility surface generated by a stochastic volatility model with jumps in returns. We use the expansion to analyse the impact on the shape of the implied volatility surface of the various features of the stochastic volatility model and to determine which stochastic volatility models are capable of reproducing the observed characteristics of the implied volatility market data.

1. Introduction

Although in principle restricted to the Black–Scholes model, implied volatility (IV thereafter) is de facto the measure by which market participants assess the relative value and quote the prices of options and other financial assets with embedded optionality. As a result, IV is an observable market quantity. Pricing models, however, are typically specified

☆ We are grateful to the Editor and two anonymous referees for very helpful comments and suggestions. We also benefited from the comments of participants at the 2017 Stanford-Tsinghua-PKU Conference in Quantitative Finance, the 2017 Fifth Asian Quantitative Finance Conference, the 2017 BCF-QUT-SJTU-SMU Conference on Financial Econometrics, the Second PKU-NUS Annual International Conference on Quantitative Finance and Economics, the 2017 Asian Meeting of the Econometric Society, the Third Annual Volatility Institute Conference at NYU Shanghai, the 2018 Review of Economic Studies 30th Anniversary Conference and the 2018 FERM Conference. The research of Chenxu Li was supported by the Guanghua School of Management, the Center for Statistical Science, and the Key Laboratory of Mathematical Economics and Quantitative Finance (Ministry of Education) at Peking University, as well as the National Natural Science Foundation of China (Grant 71671003). Chen Xu Li is grateful for a graduate scholarship and funding support from the Graduate School of Peking University as well as support from the Bendheim Center for Finance at Princeton University and the School of Business at Renmin University of China. All authors contributed equally.

* Correspondence to: Guanghua School of Management, Peking University, Beijing, 100871, PR China.
E-mail addresses: yacine@princeton.edu (Y. Aït-Sahalia), cxli@gsm.pku.edu.cn (C. Li), lichenxu@rmbs.ruc.edu.cn (C.X. Li).
1 Address: JRR Building, Princeton, NJ 08544, USA.
2 Address: School of Business, Renmin University of China, Beijing, 100872, PR China.

https://doi.org/10.1016/j.jeconom.2020.07.006
0304-4076/

in terms of the asset price's stochastic volatility (SV thereafter), which is a latent process. There exists a vast set of SV models in the literature.[3] How does one choose among them?

We propose in this paper a new method to determine whether a given SV model fits the data well. Our premise is that a successful SV model should generate IV surfaces in log-moneyness and time-to-maturity, as well as the dynamics of such surfaces, that replicate the main qualitative features of the observed market IV data: for instance, if the data suggests that the slope of the IV surface in the log-moneyness dimension has certain monotonicity properties, then the SV model should be able to reproduce such a feature.[4] Because the link between the IV surface and the SV model is not explicit, this approach necessitates additional tools. We derive explicit formulae for the shape characteristics of the IV surface generated by a given SV model. Various approximations methods for IV have been proposed.[5] Those are primarily devoted to *computing* their respective IV or option price expansions. The existing literature has not however systematically focused on *using* these expansions for the purpose of discriminating among existing models, or to try to ascertain outside very specific examples which feature(s) of SV models translate into which feature(s) of the IV surface.[6] Importantly, our formulae, unlike many existing results, are fully in closed form and, at least in principle, can be developed up to any arbitrary order by iteration. Our method is based on a bivariate series representation of the IV surface in terms of time-to-maturity and log-moneyness. As is known, the extremely short-maturity behaviour of the at-the-money IV is determined by the instantaneous SV (see, e.g., Ledoit et al., 2002 and Durrleman, 2008). This must therefore form the leading term for expanding at-the-money IV in the time-to-maturity dimension.[7] We then derive the higher order terms explicitly. One step further, we expand non-at-the-money IV in both the time-to-maturity and log-moneyness dimensions, by first expanding with respect to the log-moneyness around the at-the-money case and then expanding each term with respect to the (square root of) time-to-maturity. Our expansion applies to general SV models with jumps in returns.

A primary example in the paper consists in applying our method to the class of affine models, which are useful in practical applications since option prices can be obtained by numerical inversion of analytically tractable Fourier transforms, although their limitations in terms of fitting the data have been documented.[8] Even in the special case of affine models, explicit formulae for IV have not been available so far in the literature. Focusing on a one-factor affine SV model with jumps in returns, we examine the impact of the different model parameters on the shape of the IV surface. As we will see, the influence of the various parameters of the SV model on the IV surface is complex and varied.

We then analyse a general, not necessarily affine, bivariate SV model with jumps in returns, and study how the short-maturity behaviour of the IV shape characteristics can be explicitly related to the SV model's specification. We show how the SV and jump components control the slope of the IV smile, as well as the role that the presence of a jump term in the

[3] Earlier attempts started with the constant elasticity of variance model where the randomness of volatility is generated by the asset price itself (see, e.g., the CEV model of Cox, 1975), as well as a generalization to local volatility models (see, e.g., Dupire, 1994). Self-driven SV models include one-factor models (see e.g., Hull and White, 1987, Scott, 1987, Nelson, 1990, Stein and Stein, 1991, and Heston, 1993); two-factor models (such as Bates, 2000; Chernov et al., 2003, Christoffersen et al., 2009, Egloff et al., 2010, and Aït-Sahalia et al., 2019 among others). Modelling a continuous (stochastic) IV is sometimes done directly, see, e.g., Schönbucher (1999), Ledoit et al. (2002), Aït-Sahalia et al. (2015), and Carr and Wu (2016). Early examples of SV models with jumps in returns can be found in, e.g., Bates (1996), Bakshi et al. (1997) and Bates (2000), and with jumps in volatility in Duffie et al. (2000) and Eraker et al. (2003). Models with three factors featuring SV and/or jumps can be found in, e.g., Andersen et al. (2015), and Bardgett et al. (2019). In rough volatility models, the SV is driven by a fractional Brownian motion with Hurst index less than 1/2 (see, e.g., Fukasawa, 2011b).

[4] This approach is consistent with the one adopted for the more restrictive local volatility models in Dupire (1994), who derived the local volatility function produced by a set of option prices. This is also not unlike choosing among interest rate models based on whether they are capable of generating a desired shape of the term structure of interest rates: if one consistently observes hump-shaped term structures in the data, but the model can only generate monotonic term structures, or if the model implies that all term structure shifts are level shifts, but the data consistently exhibits more complex patterns, then the model is not a good fit for the data.

[5] By using singular perturbation techniques, Hagan and Woodward (1999) proposed an expansion for a CEV local volatility model around the local volatility evaluated at the strike of the target IV. One-dimensional expansions with respect to time-to-maturity based on the theory of large deviations have been derived in, e.g., Berestycki et al. (2004), Chapter 5 of Henry-Labordère (2008), Forde et al. (2012), and Gatheral et al. (2012), among others. This approach rarely yields closed-form expressions and the derivation of the expansion terms relies on numerical methods, except for the leading term or relatively simple and specific models. Medvedev and Scaillet (2007) obtained a univariate expansion with respect to the square root of the time-to-maturity up to the second order under one-factor jump–diffusion SV models; the expansion terms are sorted based on the moneyness degree defined as a measure of time-scaled moneyness. Expansions with respect to small volatility-of-volatility or small-diffusion have been derived in Kunitomo and Takahashi (2001), Fouque et al. (2003), Benhamou et al. (2010), Fukasawa (2011b) and Takahashi and Yamada (2012). Fouque et al. (2016) proposed a bivariate expansion for two-factor multiscale models with respect to the intrinsic time-scales of the fast-varying and the slow-varying volatility processes. Other approximations and methods can be found in Fukasawa (2011a) for an expansion of option price around the Black–Scholes price in light of an Edgeworth expansion for ergodic diffusions, Kristensen and Mele (2011) who expand intractable models around auxiliary ones, Gao and Lee (2014) for an asymptotic expansion with respect to large strikes, Xiu (2014) for a Hermite polynomial-based expansion, Lorig et al. (2017) based on polynomial expansions of the infinitesimal generator of the model, and Todorov (2019) for approximating a short-maturity portfolio of near-the-money options. Andersen and Lipton (2013) survey some of the existing methods.

[6] Examples exist, but they are to the best of our knowledge specific to the analysis of specific models and/or shape, e.g., slope of the IV surface in the log-moneyness dimension under bivariate SV models without jumps in Chapters 3 and 7 of Gatheral (2006), and IV term structure under a general class of stochastic volatility models with jumps in Fukasawa (2011b); see also Fukasawa (2017).

[7] This result holds both for continuous SV models and for models with jumps in returns. Though adding jumps to volatility can in principle improve fitting the time-series properties of the asset price and volatility, the presence of jumps in the specification of the volatility dynamics alters significantly the mathematical approach we employ. Therefore, in this paper, we focus on general SV models with jumps in returns but not in volatility.

[8] See, e.g., Jones (2003), Chernov et al. (2003), and Aït-Sahalia and Kimmel (2007).

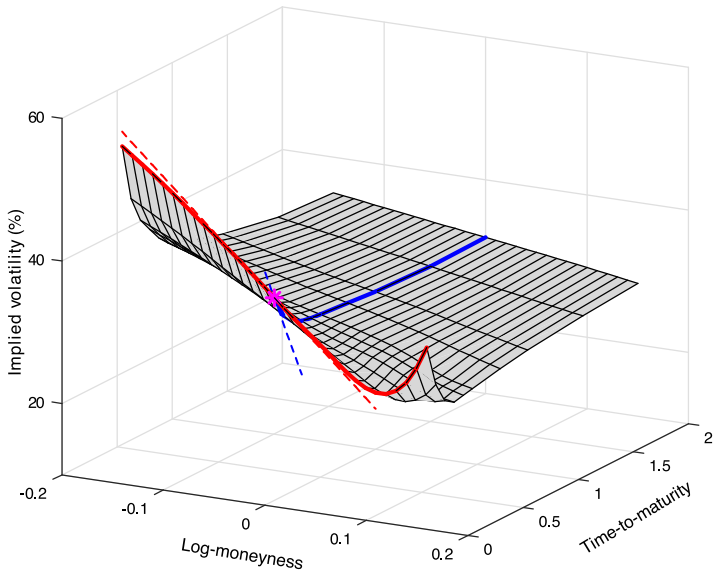

Fig. 1. The IV surface of S&P 500 index's options on May 20, 2010. Note: This figure plots the full IV surface on May 20, 2010, a representative day in the sample. The one-month (resp. at-the-money) IV curve on that day is highlighted in red (resp. blue) with the red (resp. blue) dashed line illustrating the one-month at-the-money slope along the log-moneyness (resp. time-to-maturity) dimension. The intersection of these two cross-sectional curves corresponds to the one-month at-the-money IV and is marked by a star. (For interpretation of the references to colour in this figure legend, the reader is referred to the web version of this article.)

SV model plays in generating explosive IV convexity as the time-to-maturity approaches to zero. More specifically, we show that the leverage effect parameter (defined as the generally negative correlation between the Brownian innovations to the returns and volatility dynamics), as well as the intercept and the slope parameters of the linear stochastic intensity all linearly enter into the leading order term of the at-the-money IV slope along the time-to-maturity dimension. We provide an explicit formula for the slope of the IV in the log-moneyness dimension as a function of the specification of the leverage effect and the jump intensity in the SV model.

Using these formulae, we examine which existing SV model(s) in the literature are capable of reproducing the important empirical features we observe in the IV data. We start with one-factor continuous SV models and show that different SV specifications can be employed to reproduce different IV features, but none seems to be able to match all the observed features of the IV surface. We finally examine the benefits of adding a second volatility factor to the SV model, and of further adding jumps in the returns dynamics. In a companion paper (Aït-Sahalia et al., 2020), we take the reverse approach: instead of taking existing models and determining whether they fit the data well, or where they fail to capture features of the options data, we directly construct "implied stochastic volatility models" whose coefficient functions have been designed to reproduce the characteristics of the observed IV surface.

The paper is organized as follows. We start in Section 2 by describing some of the main empirical features of IV surfaces and establishing some representative stylized facts that we then seek to reproduce using a SV model with or without jumps. Section 3 develops our closed-form expansion of the shape of the IV surface as functions of the specification of the SV model with jumps. Section 4 specializes the main results to the case of a generic bivariate SV model with jumps and explains the short-maturity behaviour of some observable shape characteristics. A more concrete example for elaborating and verifying the impact of parameters in the one-factor affine SV model with jumps is provided at the end of this section. In Section 5, we examine whether prevalent SV models with or without jumps are able to generate IV surfaces that are compatible with the stylized facts documented in Section 2. Using our explicit formulae, we ask in particular whether a second stochastic variable (resulting in a trivariate model) or a jump component (resulting in a SV model with jumps) is necessary and what part(s) of the IV surface it can help fit that one-factor models could not. Section 6 concludes. Further technical material can be found in an online supplement containing closed-form expansions under a general SV with jumps model, expansion formulae for six representative models, a verification of the accuracy of our IV expansion, a comparison with alternative expansions, some regularity assumptions for our expansion, proofs, and a smoothing procedure to employ when the regularity conditions are not satisfied in a given model. We label and cross-refer to the sections, theorems, propositions, lemmas, assumptions, and figures appearing in the online supplement with the prefix "S" to distinguish them from those of the present text.

2. Some stylized facts about IV

We start by establishing some empirical stylized facts about IV surfaces, in order to provide a target for a SV model to reproduce. The data we use consist of daily observations of IV from S&P 500 index options covering the period January 3,

Table 1
Descriptive statistics for the S&P 500 index IV data, 2005–2017.

Panel A: Number							
Log-moneyness	$< -5\%$	$[-5\%, -2.5\%)$	$[-2.5\%, 0)$	$[0, 2.5\%)$	$[2.5\%, 5\%)$	$\geq 5\%$	Total
Days-to-Expiration							
< 30	13,097	43,131	74,035	45,764	5,418	1,020	182,465
30	1,674	5,882	12,932	15,469	4,254	778	40,989
60	4,537	6,166	9,319	11,255	7,447	2,265	40,989
91	6,699	5,461	7,462	8,854	8,244	4,269	40,989
Panel B: Mean							
Log-moneyness	$< -5\%$	$[-5\%, -2.5\%)$	$[-2.5\%, 0)$	$[0, 2.5\%)$	$[2.5\%, 5\%)$	$\geq 5\%$	Total
Days-to-Expiration							
< 30	27.81	17.35	13.58	12.14	18.70	34.11	15.40
30	33.32	19.84	15.17	13.40	18.00	31.92	16.52
60	26.12	18.37	15.55	13.88	14.59	24.24	16.99
91	24.04	18.29	15.88	14.60	13.91	20.58	17.35
Panel C: Standard deviation							
Log-moneyness	$< -5\%$	$[-5\%, -2.5\%)$	$[-2.5\%, 0)$	$[0, 2.5\%)$	$[2.5\%, 5\%)$	$\geq 5\%$	Total
Days-to-Expiration							
< 30	11.96	6.12	5.62	6.08	9.21	14.25	7.94
30	11.19	6.78	5.75	5.83	6.87	9.95	7.99
60	9.36	6.04	5.30	5.48	5.86	8.65	7.54
91	8.41	5.89	4.87	5.42	5.35	8.08	7.23

Note: The sample consists of daily IV of European options written on the S&P 500 index covering the period of January 3, 2005–December 29, 2017. The means (resp. standard deviations) in Panel B (resp. C) are reported as percentages. The log-moneyness k is defined by $k = \log(K/S_t)$, where K is the exercise strike of the option and S_t the spot price of the S&P 500 index.

Table 2
Shape characteristics and their calculations.

Shape characteristic	Calculation
Level	At-the-money IV
Slope	At-the-money slope of fitted IV curve with respect to log-moneyness
Convexity	At-the-money convexity of fitted IV curve with respect to log-moneyness
Term-structure slope	At-the-money slope of fitted IV curve with respect to time-to-maturity

Note: Third-order polynomial regressions to fit IV curves along log-moneyness are employed to define the level, slope, and convexity of the IV surface. Consider for example the slope: it is calculated by differentiating the fitted polynomial with respect to log-moneyness and then evaluating this derivative at zero. Likewise, to compute the IV term-structure slope, we employ second-order polynomials to fit at-the-money IV with time-to-maturities equal to one, two, and three month(s).

2005 to December 29, 2017, obtained from OptionMetrics. We employ the fitted IV surface with time-to-maturity equal to one, two, and three month(s), as well as the raw IV data with time-to-maturity within one month. Table 1 reports the basic descriptive statistics of the sample of 305,432 observations. Table 1 divides the data into four (calendar) days-to-expiration categories and six log-moneyness categories. For each category, we report the total number, mean, and standard deviation of the IV data. As an illustration, Fig. 1 shows the full IV surface on May 20, 2010 — a representative day in our sample. In particular, the one-month (resp. at-the-money) IV curve on that day is highlighted in red (resp. blue) with the red (resp. blue) dashed line illustrating the one-month at-the-money slope along the log-moneyness (resp. time-to-maturity) dimension. The intersection of these two cross-sectional curves corresponds to the one-month at-the-money IV and is marked by a star.

In what follows, we focus on the short-maturity at-the-money level, slope, convexity, and term-structure slope as summary statistics of the IV surface.[9] Table 2 gives the precise definitions we use for these quantities. We focus on the following four stylized facts:

Stylized fact 1: Various patterns of correlations between the one-month level and slope. We provide in Fig. 2 scatter plots of one-month at-the-money level versus slope (as defined in Table 2) for four different choices of samples corresponding to different time spans: the year(s) 2005–2017, 2010, 2016, and 2017. As seen from the upper left (resp. lower right) panel,

[9] The literature has documented various empirical features of option IV, starting with the well-known skew or smile and the dependence of the slope on time-to-maturity (see Aït-Sahalia and Lo, 1998), the mean-reversion time-series behaviour of short-maturity at-the-money IV, as well as the negative correlation between changes in IV and log-returns; Carr and Wu (2003) observed that the IV smile plotted against the standardized moneyness steepens slightly as the time-to-maturity increases; Cont and da Fonseca (2002) found that the time series of the first principal component of the IV surface is persistently autocorrelated and can be fitted by an AR(1) model; Mixon (2009) summarized some stylized facts on the relationship between IV and realized volatility.

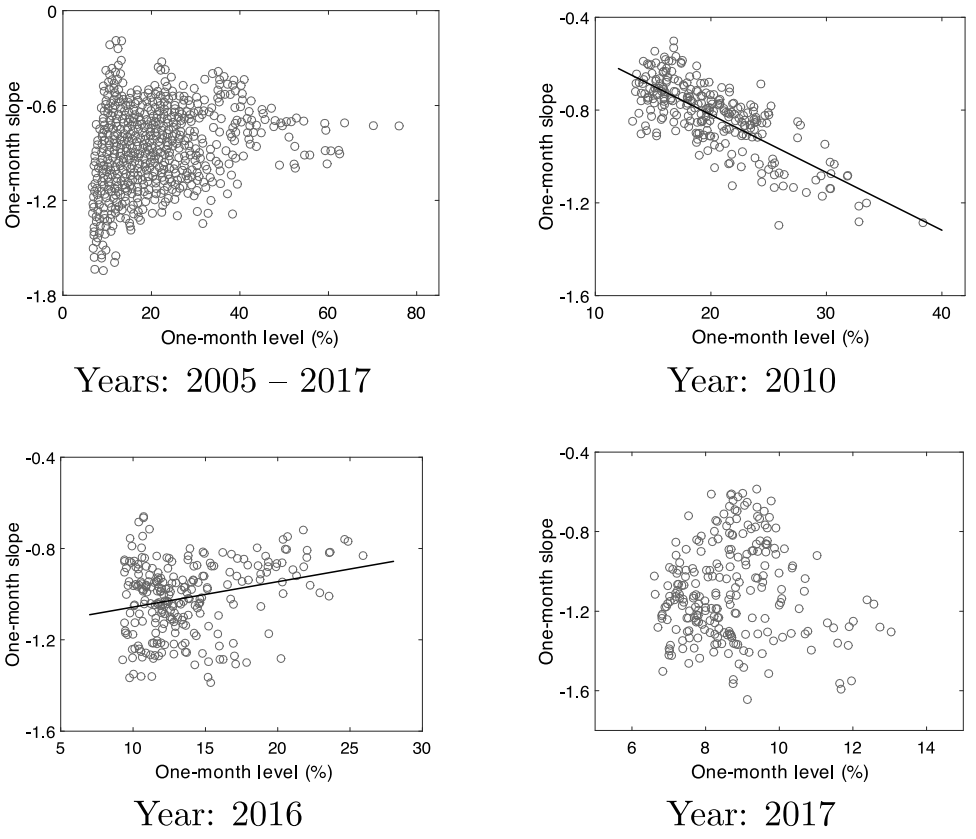

Fig. 2. Various patterns of correlation between the one-month level and slope. Note: The four panels plot for one-month level versus slope (calculated according to method clarified in Table 2) for four different choices of samples corresponding to different time spans: the year(s) of 2005–2017, 2010, 2016, and 2017. Moreover, we fit the data in the upper right and lower left panels by linear regressions slope $_t = a + b\times$ level $_t + \epsilon_t$ as shown by the solid lines, respectively. The coefficient b is estimated as -2.4883 (resp. as 1.1086) for the upper right panel (resp. for the lower left panel).

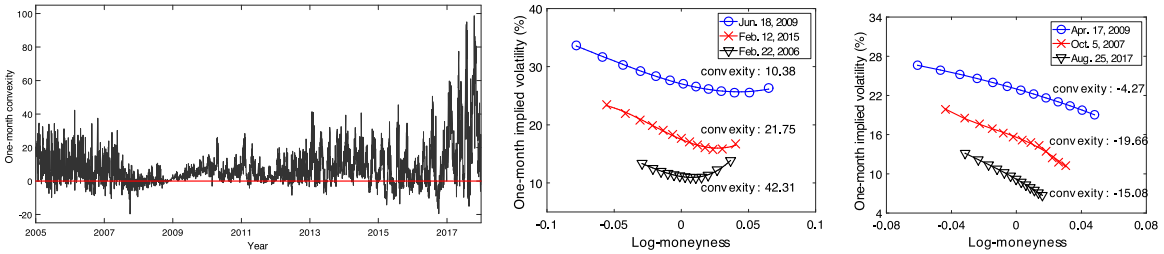

Fig. 3. Evidence of flexible sign of local convexity. Note: The left panel plots the time series of one-month at-the-money convexity from January 3, 2005 to December 29, 2017, with a red line indicating zero convexity. The middle (resp. right) panel plots one-month IV curves with positive (resp. negative) at-the-money convexities for three representative days with low, medium, and high overall IV. As a robustness check, we verified that replacing the third order polynomial in fitting the IV curves as illustrated in the note of Table 2 by a second order polynomial and/or extending the range of log-moneyness over which the regression is run from $[-0.02, 0.02]$ to $[-0.05, 0.05]$ does not meaningfully change the fact that there are days where local concavity of the IV surface occurs near the origin.

the level and slope of the entire sample (resp. of the subsample for the year 2017) are nearly uncorrelated.[10] However, on the contrary, according to the upper right (resp. lower left) panel, the level and slope in the year 2010 (resp. 2016) exhibit significantly negative (resp. positive) correlation, as shown by the linear fit. Can the same SV model generate these different patterns? A comparative analysis regarding this issue will be conducted in Section 5.

[10] Instead of exactly focusing on the short-maturity at-the-money version considered above, empirical evidence of the uncorrelation between "average" level and slope spanning the whole IV surface can be found in Christoffersen et al. (2009). It turns out that the empirical uncorrelation is not only an average effect but also a potentially local one, as discussed here, which will facilitate our comparative analysis in Section 5.

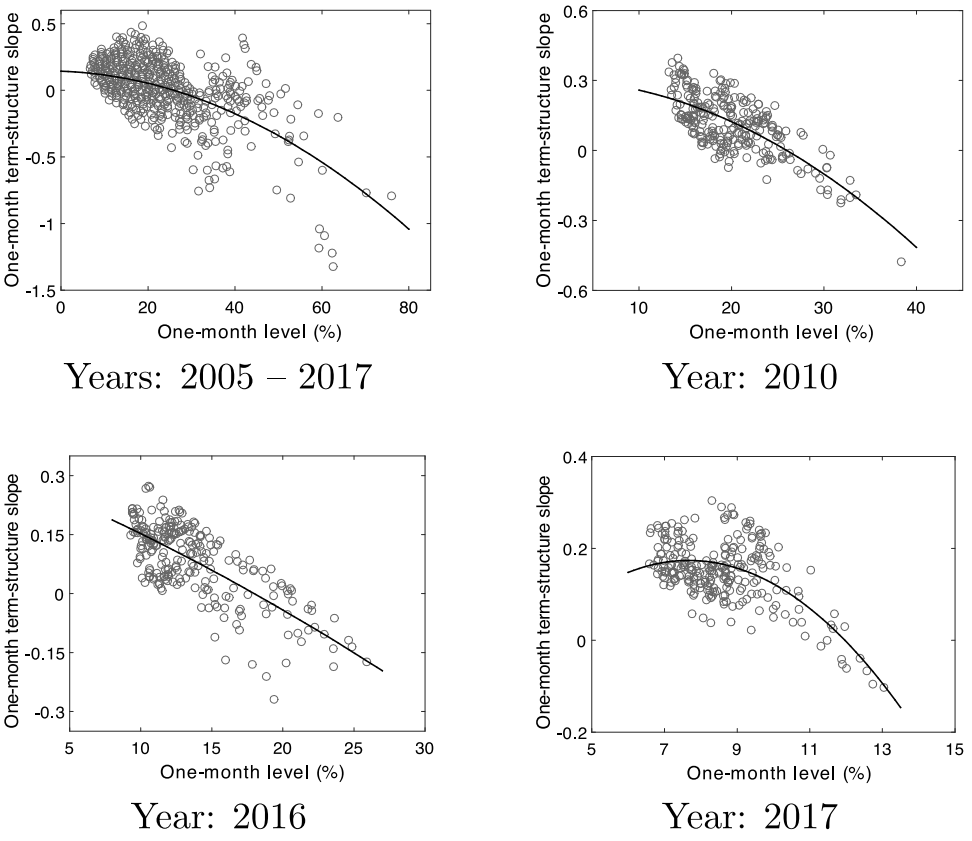

Fig. 4. Negative correlation between one-month level and term-structure slope. Note: The four panels plot for one-month at-the-money level versus term-structure slope (calculated according to the method described in Table 2) for four different choices of samples corresponding to different subsamples: the year(s) 2005–2017, 2010, 2016, and 2017. In each panel, we fit the data by a quadratic regression term-structure $\text{slope}_t = a + b\times\text{level}_t + c\times\text{level}_t^2 + \epsilon_t$ as shown by the solid curve. The coefficients a, b, and c are estimated as 0.14, −0.11, and −1.72 for the upper left panel, 0.30, −0.0053, and −4.482 for the upper right panel, 0.31, −1.47, and −1.59 for the lower left panel, as well as −0.38, 14.4, and −94.1 for the lower right panel.

Stylized fact 2: Flexible sign of local convexity. Intuitively, the IV curve for a fixed time-to-maturity is convex almost everywhere along the log-moneyness. However, the time series of one-month at-the-money convexities plotted in the left panel of Fig. 3 demonstrates the presence of negative local convexity. Hence, there is a need for a model allowing a flexible sign of the local convexity. For illustrations, the middle (resp. right) panel exhibits one-month IV curves with positive (resp. negative) local convexity on three representative days with low, medium, and high overall IV levels.

Stylized fact 3: Negative correlation between one-month level and term-structure slope. Similar to Fig. 2 for *Stylized fact 1*, we provide in Fig. 4 scatter plots of one-month at-the-money IV level versus term-structure slope for four different choices of samples corresponding to different time spans: the year(s) 2005–2017, 2010, 2016, and 2017. As a common pattern in all these four panels, the one-month level and term-structure slope are negatively correlated. More precisely, the term-structure slope tends to be positive for low volatility levels and negative for high levels. It implies that the at-the-money IV is upward sloping and downward sloping for low and high levels, respectively, and mean-reverts towards the centre as the time-to-maturity increases. Matching this pattern will prove to be possible for various SV models subject to particular constraints on model parameters.

Stylized fact 4: Possible explosion of extremely short-maturity convexity. For comparison purposes, Fig. 5 reports the box plots of level, slope, and convexity for various time-to-maturities within one month. Take the upper panel for level as an example. For each time-to-maturity τ, we collect the data of levels (as defined in Table 2) across the full sample and discard extreme values below the 5% quantile and above the 95% quantile. Then, we draw a box plot to describe the distribution of the data. As seen from the upper (resp. middle) panel, the ranges of levels (resp. slopes) remain at the same magnitude for all the time-to-maturities. However, as shown in the lower panel of Fig. 5, the range of convexities has a trend to diverge towards the positive infinity, as time-to-maturity shrinks to zero. In the left panel of Fig. 6, we

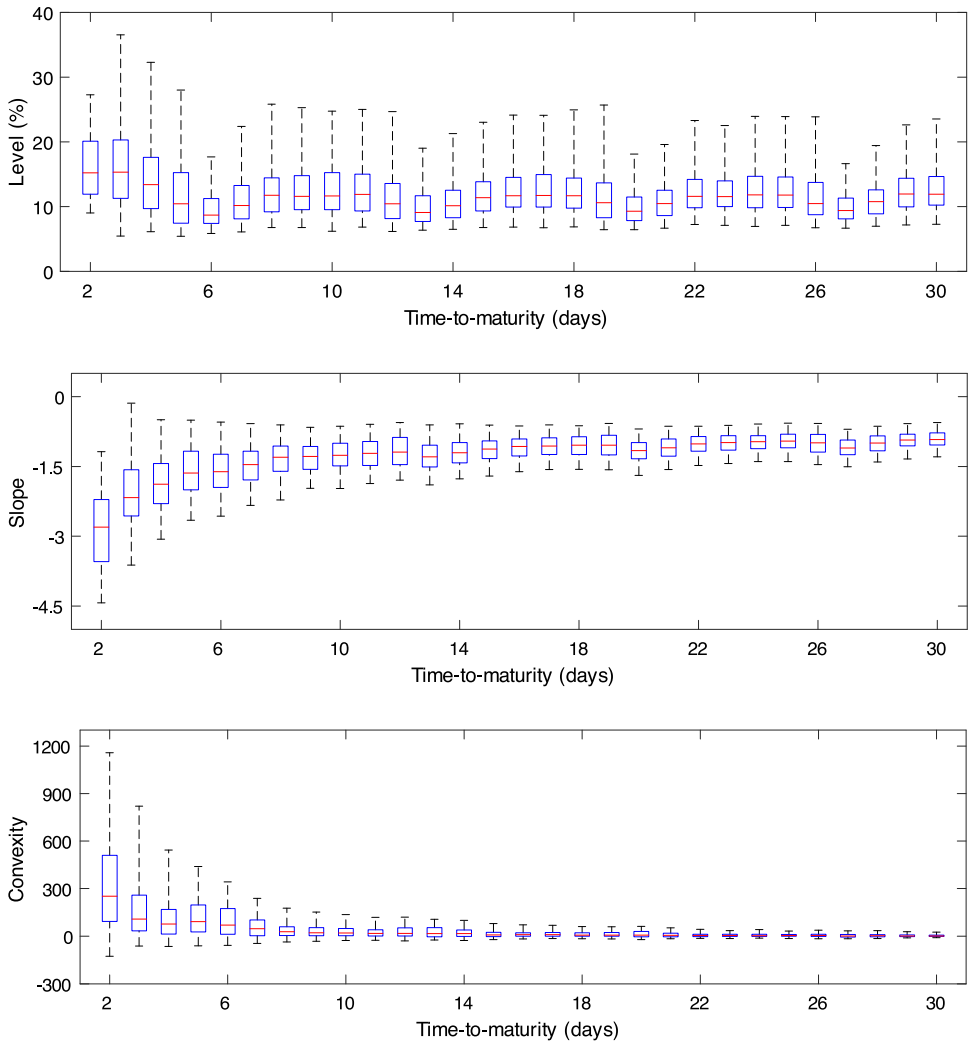

Fig. 5. Box plots of level, slope, and convexity along time-to-maturity. Note: From top to bottom, the three panels exhibit box plots of at-the-money levels, slopes, and convexities along time-to-maturity across the full sample. Take the upper panel as an illustrative example. For each time-to-maturity τ between 2 and 30 calendar days, we calculate the at-the-money level of each IV curve with time-to-maturity τ according to the method clarified in Table 2, and discard extreme values below the 5% quantile and above the 95% quantile. Then, to describe the distribution of the data, we draw a box plot to summarize the range, the first and third quartiles, as well as the median, by using the short bars at the ends of two whiskers, the upper and lower edges of the blue box, as well as the red bar inside the box, respectively.

provide a scatter plot of at-the-money convexities versus time-to-maturity for a subsample spanning February 13, 2017 to March 9, 2017. These scatter points are fitted by a nonlinear regression in the form of

$$\text{convexity}_i = a\tau_i^b + c + \epsilon_i, \tag{1}$$

where τ_i and ϵ_i represent the ith annualized time-to-maturity and observation error, respectively. The least square estimators of the three coefficients are given by $\hat{a} = 45.9$, $\hat{b} = -0.448$, and $\hat{c} = -132.9$, respectively. The positiveness of $\hat{a}$ and the negativeness of $\hat{b}$ suggest a positive explosive trend of convexity as the time-to-maturity τ approaching to zero. Although being frequently observed, the explosion of convexity is not a universal stylized fact in all subsamples. For example, as shown in the right panel of Fig. 6, the subsample spanning October 5, 2016 to October 18, 2016 suggests a nonexplosive convexity as the time-to-maturity shrinks to zero. Whether the same SV model can reproduce both patterns for convexity is one of the questions that we seek to answer.

This brief description of the data is not meant to be exhaustive, nor to suggest that those are universal features of options data. It merely seeks to motivate the need for a better understanding of whether and how various SV models are capable of giving rise to complex stylized facts concerning the shape characteristics of the IV surface. The most direct way to answer this question is to develop an explicit mapping between the functional form and parameters of the SV model and the features of the IV surface, which we will then use to assess existing models.

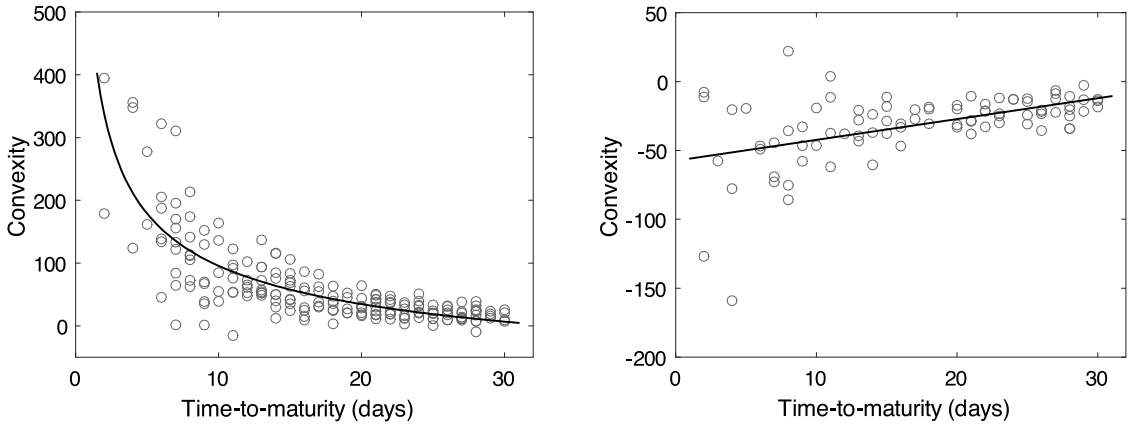

Fig. 6. Convexity versus time-to-maturity during two representative periods of time. Note: The left panel shows at-the-money convexities with time-to-maturities $\tau \leq 30$ calendar days, from February 13, 2017 to March 9, 2017. We fit the data by the nonlinear regression (1). The coefficients a, b, and c are estimated as 45.9, −0.45, and −132.9, which suggest a positively explosive trend of convexity as the time-to-maturity τ shrinks to zero. The right panel shows at-the-money convexities from October 5, 2016 to October 18, 2016. We fit the data by a linear regression $\text{convexity}_i = a + b\tau_i + \epsilon_i$. The coefficients a and b are estimated as −57.5 and 545.0, which, on the contrary, suggest a nonexplosive trend of convexity as the time-to-maturity shrinks to zero.

3. Explicitly linking a SV model and the IV surface

3.1. Notation

We consider SV models of the following form. Under an assumed risk-neutral measure, the càdlàg price of the underlying asset S_t and its m-dimensional volatility/jump intensity factor(s) X_t follows a jump–diffusion process

$$\frac{dS_t}{S_{t-}} = (r - d - \lambda(X_t)\bar{\mu})dt + v(X_t)dW_t + (\exp(J_t) - 1)dN_t, \tag{2a}$$

$$dX_t = \mu(X_t)dt + \sigma(X_t)dW_t. \tag{2b}$$

Here, r and d are the risk-free rate and the dividend yield of the underlying asset, both assumed constant for simplicity. W_t is an n-dimensional standard Brownian motion. v is an n-dimensional row vector-valued function. μ is an m-dimensional column vector-valued function. σ is an $m \times n$ matrix-valued function. For example, the first entry of the X_t will be $X_{1t} = V_t$, and play the role of the (stochastic) volatility of S_t. The next variable(s), if present, may represent for instance the stochastic level to which V_t mean-reverts, and so on. Note that this framework excludes rough volatility models, where volatility is driven by a fractional Brownian motion.

As for the jumps, N_t represents a Cox process, also known as a doubly stochastic Poisson process, with stochastic intensity $\lambda(X_t)$; N_t reduces to a standard Poisson process when its intensity is constant. J_t represents the size of log-price jump at t, if any, and is assumed to have a sufficiently smooth probability density function f and to be independent with the asset price S_t, the volatility/jump intensity factor(s) X_t, and the process N_t. When a jump occurs at time t, the log-price $\log S_t$ changes according to $\log S_t - \log S_{t-} = J_t$, i.e., $S_t - S_{t-} = (\exp(J_t) - 1)S_{t-}$. Define

$$\bar{\mu} = \mathbb{E}[\exp(J_t)] - 1, \tag{3}$$

where $\mathbb{E}$ denotes the risk-neutral expectation. The drift term $-\lambda(X_t)\bar{\mu}dt$ compensates the jump component $(\exp(J_t)-1)dN_t$ in order to make the process $\int_0^t (\exp(J_s) - 1)dN_s - \int_0^t \lambda(X_s)\bar{\mu}ds$ a martingale under the risk-neutral measure.[11]

The arbitrage-free price of an European-style put option with maturity T, i.e., time-to-maturity $\tau = T - t$, and exercise strike K is, in terms of log-moneyness $k = \log(K/S_t)$,

$$P(\tau, k, S_t, X_t) = e^{-r\tau}\mathbb{E}_t[\max(S_t e^k - S_T, 0)], \tag{4}$$

where $\mathbb{E}_t$ denotes the risk-neutral conditional expectation given the information up to time t. The Black–Scholes price of the option is

$$P_{\text{BS}}(\tau, S_t, K, \sigma) = S_t \bar{P}_{\text{BS}}(\tau, \log(K/S_t), \sigma) \text{ with } \bar{P}_{\text{BS}}(\tau, k, \sigma) = e^{k-r\tau}\mathcal{N}(-d_2) - e^{-d\tau}\mathcal{N}(-d_1), \tag{5}$$

[11] This setup nests many existing SV models with jumps in returns considered in the literature, e.g., Bates (1996), (Duffie et al., 2000), Pan (2002) and Aït-Sahalia et al. (2019), among others. By letting the jump intensity function $\lambda(x)$ be zero in model (2a)–(2b), we obtain a continuous SV model, which nests all existing continuous SV models. As already noted, jumps in the volatility dynamics (2b) are excluded.

$$d_1 = \frac{1}{\sigma\sqrt{\tau}}\left[-k + \left(r - d + \frac{1}{2}\sigma^2\right)\tau\right] \text{ and } d_2 = \frac{1}{\sigma\sqrt{\tau}}\left[-k + \left(r - d - \frac{1}{2}\sigma^2\right)\tau\right].$$

with $\mathcal{N}$ denoting the cumulative distribution function of the standard normal distribution.

In practice, the market price of an option is typically quoted through its Black–Scholes IV, i.e., the value of the volatility parameter which, when plugged into the Black–Scholes formula, leads to a theoretical value equal to the observed market price of the option. Using the monotonicity property of formula (5) with respect to the volatility parameter σ, the model IV Σ is the unique root of the equation $P_{\text{BS}}(\tau, S_t, S_t e^k, \Sigma) = P(\tau, k, S_t, X_t)$. It is straightforward to verify that the IV Σ depends on τ, k, as well as X_t, and thus can be written in as a function $\Sigma(\tau, k, X_t)$. Indeed, it follows from (4) that

$$P(\tau, k, S_t, X_t) = S_t \bar{P}(\tau, k, X_t) \text{ with } \bar{P}(\tau, k, X_t) = e^{-r\tau}\mathbb{E}_t\left[\max\left(e^k - \frac{S_T}{S_t}, 0\right)\right]. \tag{6}$$

For a given log-moneyness k, the function $\bar{P}(\tau, k, X_t)$ is independent with the initial underlying asset price S_t since (2a) implies

$$\frac{S_T}{S_t} = \exp\left\{\int_t^T \left(r - d - \lambda(X_s)\bar{\mu} - \frac{1}{2}\sum_{i=1}^{n} v_i(X_s)^2\right) ds + \int_t^T v(X_s) dW_s + \sum_{i=N_t+1}^{N_T} J_{\tau_i}\right\}, \tag{7}$$

with τ_i denoting the ith jump arrival time. The ratio S_T/S_t is independent of S_t, hence so is the expectation function (6) for defining $\bar{P}(\tau, k, X_t)$. Therefore, the IV Σ is essentially determined by

$$\bar{P}_{\text{BS}}(\tau, k, \Sigma) = \bar{P}(\tau, k, X_t), \tag{8}$$

where the functions $\bar{P}$ and $\bar{P}_{\text{BS}}$ are given in (6) and (5), respectively. The mapping $(\tau, k) \longmapsto \Sigma(\tau, k, X_t)$ at a given t is the (model) IV surface at that time. The model IV's calculated from put and call options are identical due to put–call parity. The various shape characteristics of the IV surface (for example, level, slope, and convexity along either the moneyness dimension or the term-structure dimension) discussed in Section 2 have model counterparts characterized by the model IV and its sensitivities

$$\Sigma_{i,j}(\tau, k, X_t) := \frac{\partial^{i+j}\Sigma}{\partial\tau^i \partial k^j}(\tau, k, X_t),$$

for integers $i, j \geq 0$.

3.2. Structure of the expansion of the shape characteristics of the IV surface

To proceed with the computation of our expansion, we make, in addition to the regularity conditions given in Section S.5, the following main assumption.

Assumption 1. Replacing time-to-maturity τ (resp. log-moneyness k) in $\Sigma(\tau, k, X_t)$ by ϵ^2 (resp. $k'\epsilon$), we consider the following equivalent form of IV $\Sigma'(\epsilon, k', X_t) := \Sigma(\epsilon^2, k'\epsilon, X_t)$. For integers $K_1, K_2 \geq 0$, the IV $\Sigma'(\epsilon, k', X_t)$ is differentiable $K_1 + 1$ and $K_2 + 1$ times with respect to $\epsilon = \sqrt{\tau}$ and $k' = k/\epsilon$ respectively in a neighbourhood of $(\epsilon, k') = (0, 0)$ and admits the following Taylor expansion as a bivariate polynomial

$$\Sigma'^{(K_1,K_2)}(\epsilon, k', X_t) = \sum_{n_2'=0}^{K_2}\sum_{n_1'=0}^{K_1} \varphi^{(n_1', n_2')}(X_t)\epsilon^{n_1'}(k')^{n_2'}, \tag{9}$$

$$\text{where } \varphi^{(n_1', n_2')}(X_t) = \frac{1}{n_1'!n_2'!}\frac{\partial^{n_1'+n_2'}}{\partial\epsilon^{n_1'}\partial(k')^{n_2'}}\Sigma'(0, 0, X_t). \tag{10}$$

This assumption states that, on the one hand, in terms of ϵ and k', the IV expansion involves no singularity (i.e., no negative powers of ϵ and k'). A bivariate expansion of $\Sigma_{i,j}(\tau, k, X_t)$, for integers $i, j \geq 0$[12] along the time-to-maturity and log-moneyness, can be directly obtained by replacing k' as k/ϵ in expansion (9) and then differentiating this expansion with respect to k and $\tau = \epsilon^2$ for j and i times, respectively:

$$\Sigma_{i,j}^{(J_1,J_2)}(\tau, k, X_t) = \sum_{n_2=0}^{J_2}\sum_{n_1=L_{n_2}^{(i,j)}}^{J_1} \sigma_{i,j}^{(n_1,n_2)}(X_t)\epsilon^{n_1}k^{n_2}. \tag{11}$$

The expansion in terms of ϵ and k, on the other hand, will typically involve a singularity. For arbitrary $n_2 \geq 0$, $L_{n_2}^{(i,j)}$ is a (finite but possibly negative) constant integer, and represents the lowest power of ϵ in the nonzero terms of order

[12] When there is no risk of confusion, we write $\Sigma \equiv \Sigma_{0,0}$.

$\epsilon^{n_1}k^{n_2}$; it depends on n_2, i, and j. The key here is that $L_{n_2}^{(i,j)}$ is finite. For example for $i=j=0$, we determine the index lower bound $L_{n_2}^{(0,0)} \equiv L_{n_2}$ and the expansion terms $\sigma_{0,0}^{(n_1,n_2)}(X_t) \equiv \sigma^{(n_1,n_2)}(X_t)$ by matching orders with respect to $\epsilon = \sqrt{\tau}$ and k of the Black–Scholes price evaluated at the expansion and the price under model (2a)–(2b). The expansion for $i \geq 1$ or $j \geq 1$ can be obtained by formal differentiation of (11) for $i=j=0$. Since the bivariate Taylor expansion (9) for IV Σ' converges locally as $(\epsilon, k') \to (0,0)$, we interpret the convergence of the resulting IV expansion in the form (11) as $k = o(\epsilon)$ and $\epsilon \to 0$ in light of $k' = k/\epsilon$. In the case of continuous SV models, $L_{n_2}^{(i,j)} = 0$ for all $i, j \geq 0$. Primitive conditions that imply Assumption 1 are not easily available. However, we show in the next section that Assumption 1 is satisfied in the important case of the jump–diffusion model of Merton (1976).

3.3. The expansion in the Merton model as an illustration

We now illustrate how to construct our expansion for the jump–diffusion model of Merton (1976), where

$$\frac{dS_t}{S_{t-}} = (r - d - \lambda\bar{\mu})dt + \gamma dW_t + (\exp(J_t) - 1)dN_t.$$

The parameters $\gamma > 0$ and $\lambda > 0$ describe the constant volatility and the constant intensity of Poisson process N_t, respectively; the jump size J_t is normally distributed with mean μ_J and variance σ_J^2, so that the jump compensator is $\bar{\mu} = \exp(\mu_J + \sigma_J^2/2) - 1$. Following (6) for the general model (2a)–(2b) and the fact that $X_t = \gamma$, the option price is

$$\bar{P}(\tau, k, \gamma) = \sum_{n=0}^{\infty} e^{-\lambda\tau}\frac{(\lambda\tau)^n}{n!}\left[e^{k-r\tau}\mathcal{N}(-d_{2,n}) - e^{-(d+\lambda\bar{\mu})\tau}(\bar{\mu}+1)^n\mathcal{N}(-d_{1,n})\right], \tag{12}$$

where $d_{1,n} = d_{2,n} + \sqrt{\gamma^2\tau + n\sigma_J^2}$ and $d_{2,n} = \dfrac{1}{\sqrt{\gamma^2\tau + n\sigma_J^2}}\left[-k + \left(r - d - \lambda\bar{\mu} - \dfrac{1}{2}\gamma^2\right)\tau + n\mu_J\right]$.

We first verify that Assumption 1 is satisfied by this model, proceeding as follows. We construct a trivariate function $f(\epsilon, k', \sigma)$ satisfying differentiability and nondegeneracy conditions, such that $\Sigma'(\epsilon, k', \gamma)$ is implicitly determined via equation $f(\epsilon, k', \Sigma'(\epsilon, k', \gamma)) = 0$. Then, applying the implicit function theorem, we obtain the differentiability of Σ' with respect to (ϵ, k') around $(0,0)$. The bivariate Taylor expansion (9) follows from further application of Taylor's theorem. Consider the function f defined by

$$f(\epsilon, k', \sigma) = \frac{1}{\epsilon}\left[\bar{P}'_{\mathrm{BS}}(\epsilon, k', \sigma) - \bar{P}'(\epsilon, k', \gamma)\right], \tag{13}$$

where $\bar{P}'(\epsilon, k', \gamma) = \bar{P}(\epsilon^2, \epsilon k', \gamma)$, and $\bar{P}'_{\mathrm{BS}}(\epsilon, k', \sigma) = \bar{P}_{\mathrm{BS}}(\epsilon^2, \epsilon k', \sigma)$. The function f is originally defined for any $\epsilon \in \mathbb{R}\backslash\{0\}$. We extend it as a function for all $\epsilon \in \mathbb{R}$, by letting $f(0, k', \sigma) := \lim_{\epsilon\to 0} f(\epsilon, k', \sigma)$ for any $k' \in \mathbb{R}$ and $\sigma > 0$. It follows from the expressions of $\bar{P}$ in (12) and $\bar{P}_{\mathrm{BS}}$ in (5) that the above limit is finite, and the function f by construction is infinitely differentiable with respect to ϵ, k', and σ in an open set containing $(0,0,\gamma)$ as an interior point. By direct computation, we verify that $f(0,0,\gamma) = 0$ and $\partial f(0,0,\gamma)/\partial\sigma = 1/\sqrt{2\pi} \neq 0$. Then, it follows from the implicit function theorem (see, e.g., Theorem 3.3.1 in Krantz and Parks, 2003) that $\Sigma'(\epsilon, k', \gamma)$ is infinitely differentiable with respect to (ϵ, k') around $(0,0)$. The bivariate expansion (9) follows from Taylor's theorem for multivariate functions.

Consider the expansion for the IV itself, i.e., $i=j=0$. We show how an order-matching procedure can be performed by determining the index lower bound $L_{n_2}^{(0,0)} \equiv L_{n_2}$ and expansion terms $\sigma_{0,0}^{(n_1,n_2)} \equiv \sigma^{(n_1,n_2)}$. This is done sequentially in n_2, and we show the calculations for $n_2 = 0$, 1, and 2. Eq. (8) becomes $\bar{P}_{\mathrm{BS}}(\tau, k, \Sigma(\tau, k, \gamma)) = \bar{P}(\tau, k, \gamma)$. We consider the two versions of at-the-money price sensitivities:

$$\tilde{P}_n(\epsilon, \gamma) := \frac{\partial^n}{\partial k^n}\bar{P}_{\mathrm{BS}}(\epsilon^2, k, \Sigma(\epsilon^2, k, \gamma))\Big|_{k=0} \quad \text{and} \quad \bar{P}_n(\epsilon, \gamma) := \frac{\partial^n}{\partial k^n}\bar{P}(\epsilon^2, k, \gamma)\Big|_{k=0}$$

and we have, for all n,

$$\tilde{P}_n(\epsilon, \gamma) = \bar{P}_n(\epsilon, \gamma). \tag{14}$$

The case $n_2 = 0$: We begin by determining L_0. By setting $i=j=k=J_2=0$ in the bivariate expansion (11), we obtain the following J_1th order univariate expansion of the at-the-money IV $\Sigma(\epsilon^2, 0, \gamma)$ with respect to ϵ:

$$\Sigma^{(J_1,0)}(\epsilon^2, 0, \gamma) = \sum_{n_1=L_0}^{J_1} \sigma^{(n_1,0)}(\gamma)\epsilon^{n_1}. \tag{15}$$

The convergence of at-the-money IV to SV as $\epsilon \to 0$ (see, e.g., Durrleman, 2010) shows that the lowest order L_0 of ϵ must be 0 and the leading term $\sigma^{(0,0)}(\gamma)$ coincides with the spot volatility γ. Then, expansion (15) becomes the following Taylor expansion

$$\Sigma^{(J_1,0)}(\epsilon^2, 0, \gamma) = \sum_{n_1=0}^{J_1} \sigma^{(n_1,0)}(\gamma)\epsilon^{n_1}. \tag{16}$$

To solve the desired IV expansion terms $\sigma^{(n_1,0)}$, we resort to Eq. (14) for the case of $n = 0$, i.e., $\tilde{P}_0(\epsilon, \gamma) = \bar{P}_0(\epsilon, \gamma)$. By expanding both sides of the above identity with respect to ϵ, we can match the corresponding expansion terms to solve $\sigma^{(n_1,0)}$ recursively along the index n_1. Indeed, by composing the Black–Scholes formula and expansion (16), we expand the left hand side $\tilde{P}_0(\epsilon, \gamma)$ as

$$\tilde{P}_0^{(J)}(\epsilon, \gamma) = \sum_{l=1}^{J} \tilde{p}_0^{(l)}(\gamma)\epsilon^l, \tag{17}$$

where we have

$$\begin{aligned}
&\tilde{p}_0^{(1)}(\gamma) = \frac{\sigma^{(0,0)}(\gamma)}{\sqrt{2\pi}},\ \tilde{p}_0^{(2)}(\gamma) = \frac{\sigma^{(1,0)}(\gamma)}{\sqrt{2\pi}} + \frac{d-r}{2},\\
&\tilde{p}_0^{(3)}(\gamma) = \frac{1}{24\sqrt{2\pi}\sigma^{(0,0)}(\gamma)}\left[12d\left(\sigma^{(0,0)}(\gamma)^2 + 2r\right) + 12r\sigma^{(0,0)}(\gamma)^2\right.\\
&\qquad \left. + \sigma^{(0,0)}(\gamma)^4 - 24\sigma^{(2,0)}(\gamma)\sigma^{(0,0)}(\gamma) - 12(d^2 + r^2)\right].
\end{aligned}$$

On the other hand, from the option pricing formula (12), we expand the right hand side $\bar{P}_0(\epsilon, \gamma)$ in the form

$$\bar{P}_0^{(J)}(\epsilon, \gamma) = \sum_{l=1}^{J} \bar{p}_0^{(l)}(\gamma)\epsilon^l, \tag{18}$$

where we have

$$\begin{aligned}
&\bar{p}_0^{(1)}(\gamma) = \frac{\gamma}{\sqrt{2\pi}},\ \bar{p}_0^{(2)}(\gamma) = \frac{1}{2}\left(d - r - 2\lambda\mathcal{N}(\mu_-) + 2\lambda(\bar{\mu}+1)\mathcal{N}(\mu_+) - \lambda\bar{\mu}\right),\\
&\bar{p}_0^{(3)}(\gamma) = \frac{1}{24\sqrt{2\pi}\gamma}\left[\gamma^4 + 12\gamma^2\lambda\bar{\mu} + 24\gamma^2\lambda - 12d^2 + 12d\left(\gamma^2 - 2\lambda\bar{\mu} + 2r\right)\right.\\
&\qquad \left. - 12\lambda^2\bar{\mu}^2 - 12r^2 + 12r\left(\gamma^2 + 2\lambda\bar{\mu}\right)\right].
\end{aligned}$$

Here, we write

$$\mu_- = \frac{\mu_J}{\sigma_J} \text{ and } \mu_+ = \frac{\mu_J}{\sigma_J} + \sigma_J. \tag{19}$$

We now match expansion terms of (17) and (18) in order to solve the desired IV expansion terms $\sigma^{(n_1,0)}$: By equating $\bar{p}_0^{(1)}$ and $\tilde{p}_0^{(1)}$, we solve the leading term $\sigma^{(0,0)}$ as γ. Then, by equating $\bar{p}_0^{(2)}$ and $\tilde{p}_0^{(2)}$, we solve for $\sigma^{(1,0)}$ in closed form. Then, with the solved $\sigma^{(0,0)}$ and $\sigma^{(1,0)}$ as inputs, solving $\bar{p}_0^{(3)}(\gamma) = \tilde{p}_0^{(3)}(\gamma)$ leads to the closed-form formula of $\sigma^{(2,0)}$. We provide the closed-form formulae of $\sigma^{(1,0)}$ and $\sigma^{(2,0)}$ in Example 4 of Section S.2. Similarly, by equating higher order terms $\bar{p}_0^{(l)}$ and $\tilde{p}_0^{(l)}$ and taking the previously solved IV expansion terms as inputs, all higher order terms $\sigma^{(n_1,0)}$ can be solved recursively.

The case $n_2 = 1$: We now determine the lowest order L_1 and solve the IV expansion terms $\sigma^{(n_1,1)}$ based on Eq. (14) for the case of $n = 1$, i.e.,

$$\tilde{P}_1(\epsilon, \gamma) = \bar{P}_1(\epsilon, \gamma), \tag{20}$$

Here, $\bar{P}_1(\epsilon, \gamma) = \partial\bar{P}(\epsilon^2, 0, \gamma)/\partial k$ can be calculated based on (12), and $\tilde{P}_1(\epsilon, \gamma)$ can be calculated as

$$\tilde{P}_1(\epsilon, \gamma) = \frac{\partial\bar{P}_{\text{BS}}}{\partial k}(\epsilon^2, 0, \Sigma(\epsilon^2, 0, \gamma)) + \frac{\partial\bar{P}_{\text{BS}}}{\partial\sigma}(\epsilon^2, 0, \Sigma(\epsilon^2, 0, \gamma))\Sigma_{0,1}(\epsilon^2, 0, \gamma), \tag{21}$$

which includes the Black–Scholes formula (5) and its sensitivities, as well as the unknown at-the-money IV $\Sigma(\epsilon^2, 0, \gamma)$ and IV sensitivity $\Sigma_{0,1}(\epsilon^2, 0, \gamma)$.

To expand both sides of (20) and then match orders, we need the following two IV-related expansions: the first is expansion (16) of at-the-money IV $\Sigma^{(J_1,0)}(\epsilon^2, 0, \gamma)$ up to a sufficiently large order J_1, which is obtained previously under *the case* $n_2 = 0$. The second is the expansion of at-the-money IV slope $\Sigma_{0,1}(\epsilon^2, 0, \gamma)$, which is obtained from (11):

$$\Sigma_{0,1}^{(J_1,0)}(\epsilon^2, 0, \gamma) = \sum_{n_1=L_1}^{J_1} \sigma^{(n_1,1)}(\gamma)\epsilon^{n_1}. \tag{22}$$

The two expansions lead to that of (21). Matching the terms with those of the expansion of $\bar{P}_1(\epsilon, \gamma)$ from (12), we determine the value of L_1 and obtain the closed-form formulae of $\sigma^{(n_1,1)}$.

We begin by expanding $\bar{P}_1(\epsilon, \gamma)$. From (12), we have

$$\bar{P}_1^{(J)}(\epsilon, \gamma) = \sum_{l=0}^{J} \bar{p}_1^{(l)}(\gamma)\epsilon^l, \tag{23}$$

where the first three expansion terms are

$$\bar{p}_1^{(0)}(\gamma)=\frac{1}{2},\ \bar{p}_1^{(1)}(\gamma)=\frac{1}{2\sqrt{2\pi}\gamma}\left[2(d-r)+2\lambda\bar{\mu}+\gamma^2\right],\ \bar{p}_1^{(2)}(\gamma)=\frac{1}{2}\left(-2\lambda\mathcal{N}(\mu_-)+\lambda-r\right).$$

We now investigate the expansion of $\tilde{P}_1(\epsilon,\gamma)$. According to (21), the at-the-money IV expansion (16), and the at-the-money IV slope expansion (22), the lowest order in the expansion of $\tilde{P}_1(\epsilon,\gamma)$ ought to be $\min(0,1+L_1)$, by calculating the minimum of orders of the expansions of the two summands $\partial\bar{P}_{\rm BS}(\epsilon^2,0,\Sigma(\epsilon^2,0,\gamma))/\partial k$ and $\partial\bar{P}_{\rm BS}(\epsilon^2,0,\Sigma(\epsilon^2,0,\gamma))/\partial\sigma\,\Sigma_{0,1}(\epsilon^2,0,\gamma)$. Matching this lowest order with that in expansion (23) yields $L_1\geq -1$.

We now use a contradiction argument to show that $L_1=0$ and at the same time identify the desired IV expansion terms $\sigma^{(n_1,1)}$. Suppose otherwise $L_1=-1$. Then, the Jth order expansion of $\tilde{P}_1(\epsilon,\gamma)$ can be computed as

$$\tilde{P}_1^{(J)}(\epsilon,\gamma)=\sum_{l=0}^{J}\tilde{p}_1^{(l)}(\gamma)\epsilon^l, \tag{24}$$

where we have for instance the first three expansion terms as

$$\begin{aligned}
\tilde{p}_1^{(0)}(\gamma)&=\frac{1}{2}+\frac{\sigma^{(-1,1)}(\gamma)}{\sqrt{2\pi}},\\
\tilde{p}_1^{(1)}(\gamma)&=\frac{1}{2\sqrt{2\pi}\sigma^{(0,0)}(\gamma)}\left[\sigma^{(0,0)}(\gamma)^2+2\sigma^{(0,0)}(\gamma)\sigma^{(0,1)}(\gamma)+2(d-r)\right],\\
\tilde{p}_1^{(2)}(\gamma)&=\frac{1}{16\sqrt{\pi}\sigma^{(0,0)}(\gamma)^2}\left[-4\sigma^{(0,0)}(\gamma)^2\left(\sqrt{2}(\sigma^{(-1,1)}(\gamma)(d+r)-\sigma^{(1,0)}(\gamma)-2\sigma^{(1,1)}(\gamma)\right)\right.\\
&\quad\left.+2\sqrt{\pi}r\right)-4\sqrt{2}(d-r)(\sigma^{(-1,1)}(\gamma)(d-r)+2\sigma^{(1,0)}(\gamma))-\sqrt{2}\sigma^{(-1,1)}(\gamma)\sigma^{(0,0)}(\gamma)^4\Big].
\end{aligned}$$

Now, viewing $\sigma^{(0,0)}$, $\sigma^{(1,0)}$, and $\sigma^{(2,0)}$ computed from *the case* $n_2=0$ as inputs, we match the expansion terms of (23) and (24) in order to solve the desired IV expansion terms $\sigma^{(n_1,1)}$: We solve equations $\bar{p}_1^{(l)}=\tilde{p}_1^{(l)}$ for $l=0,1,2$ recursively to obtain the closed-form formulae of $\sigma^{(-1,1)}$, $\sigma^{(0,1)}$, and $\sigma^{(1,1)}$. Straightforward computations yield that $\sigma^{(-1,1)}(\gamma)\equiv 0$ while $\sigma^{(0,1)}$ and $\sigma^{(1,1)}$ are nonzero; see the closed-form formulae given in Example 4 of Section S.2. This contradicts $L_1=-1$, and therefore it must be that $L_1=0$. Similarly, all higher order terms $\sigma^{(n_1,1)}$ can be obtained recursively by equating higher order expansion terms $\bar{p}_1^{(l)}$ and $\tilde{p}_1^{(l)}$.

The case $n_2=2$: We now determine the lowest order L_2 and solve the IV expansion terms $\sigma^{(n_1,2)}$ based on Eq. (14) for the case of $n=2$, i.e.,

$$\bar{P}_2(\epsilon,\gamma)=\tilde{P}_2(\epsilon,\gamma). \tag{25}$$

Here, $\bar{P}_2(\epsilon,\gamma)=\partial^2\bar{P}(\epsilon^2,0,\gamma)/\partial k^2$ can be calculated in closed form directly based on (12), and $\tilde{P}_2(\epsilon,\gamma)$ can be calculated as

$$\begin{aligned}
\tilde{P}_2(\epsilon,\gamma)&=\frac{\partial^2}{\partial k^2}\bar{P}_{\rm BS}(\epsilon^2,0,\Sigma(\epsilon^2,0,\gamma))+2\frac{\partial^2}{\partial k\partial\sigma}\bar{P}_{\rm BS}(\epsilon^2,0,\Sigma(\epsilon^2,0,\gamma))\Sigma_{0,1}(\epsilon^2,0,\gamma)\\
&\quad+\frac{\partial^2}{\partial\sigma^2}\bar{P}_{\rm BS}(\epsilon^2,0,\Sigma(\epsilon^2,0,\gamma))\Sigma_{0,1}(\epsilon^2,0,\gamma)^2+\frac{\partial\bar{P}_{\rm BS}}{\partial\sigma}(\epsilon^2,0,\Sigma(\epsilon^2,0,\gamma))\Sigma_{0,2}(\epsilon^2,0,\gamma),
\end{aligned} \tag{26}$$

which includes the Black–Scholes formula (5) and its sensitivities, as well as the unknown at-the-money IV $\Sigma(\epsilon^2,0,\gamma)$ and two IV sensitivities $\Sigma_{0,1}(\epsilon^2,0,\gamma)$ and $\Sigma_{0,2}(\epsilon^2,0,\gamma)$.

To expand the both sides of (25) and then match orders, we naturally need the following three IV-related expansions: The first two are the expansions (16) and (22) for the at-the-money IV and at-the-money IV slope, respectively, which are assumed to be known already through *the cases* $n_2=0$ and 1. The third one is the expansion of at-the-money IV convexity $\Sigma_{0,2}(\epsilon^2,0,\gamma)$:

$$\Sigma_{0,2}^{(J_1,0)}(\epsilon^2,0,\gamma)=\sum_{n_1=L_2}^{J_1}2\sigma^{(n_1,2)}(\gamma)\epsilon^{n_1}. \tag{27}$$

These three expansions lead to that of (26). Matching the terms with those of the expansion of $\bar{P}_2(\epsilon,\gamma)$ to be calculated based on the closed-form option pricing formula (12), we determine the value of L_2 and obtain the closed-form formulae of $\sigma^{(n_1,2)}$.

We begin by expanding $\bar{P}_2(\epsilon,\gamma)$. Following the closed-form option pricing formula (12), we have

$$\bar{P}_2^{(J)}(\epsilon,\gamma)=\sum_{l=-1}^{J}\bar{p}_2^{(l)}(\gamma)\epsilon^l, \tag{28}$$

where we have for instance the first three expansion terms as

$$\begin{aligned}\bar{p}_2^{(-1)}(\gamma) &= \frac{1}{\sqrt{2\pi}\gamma},\ \bar{p}_2^{(0)}(\gamma) = \frac{1}{2},\\ \bar{p}_2^{(1)}(\gamma) &= \frac{1}{8\sqrt{2\pi}\gamma^3}\left[3\gamma^4 + 4\gamma^2\lambda\bar{\mu} - 8\gamma^2\lambda - 4d^2 + 4d\left(\gamma^2 - 2\lambda\bar{\mu} + 2r\right)\right.\\ &\quad \left. - 4\lambda^2\bar{\mu}^2 - 4r^2 - 12\gamma^2 r + 8\lambda\bar{\mu}r\right].\end{aligned}$$

Next we expand $\tilde{P}_2(\epsilon,\gamma)$. According to (26) and the three at-the-money IV-related expansions (16), (22), and (27), the lowest order in the expansion of $\tilde{P}_2(\epsilon,\gamma)$ ought to be $\min(-1, 1+L_2)$, by calculating the minimum of orders of the expansions of the summands in (26). Matching this lowest order with that in expansion (28) yields $L_2 \geq -2$. Similar to the case $n_2 = 1$, we use a contradiction argument to show that $L_2 = -1$ and at the same time identify the desired IV expansion terms $\sigma^{(n_1,2)}$. Suppose otherwise $L_2 = -2$. Then, the Jth order expansion of $\tilde{P}_2(\epsilon,\gamma)$ can be computed as

$$\tilde{P}_2^{(J)}(\epsilon,\gamma) = \sum_{l=-1}^{J} \tilde{p}_2^{(l)}(\gamma)\epsilon^l, \tag{29}$$

where we have for instance the first three expansion terms as

$$\begin{aligned}\tilde{p}_2^{(-1)}(\gamma) &= \frac{1}{\sqrt{2\pi}\sigma^{(0,0)}(\gamma)}\left[2\sigma^{(-2,2)}(\gamma)\sigma^{(0,0)}(\gamma) + 1\right],\\ \tilde{p}_2^{(0)}(\gamma) &= \frac{1}{\sqrt{2\pi}}\left(2\sigma^{(-1,2)}(\gamma) - \frac{\sigma^{(1,0)}(\gamma)}{\sigma^{(0,0)}(\gamma)^2}\right) + \frac{1}{4},\\ \tilde{p}_2^{(1)}(\gamma) &= \frac{1}{8\sqrt{2\pi}\sigma^{(0,0)}(\gamma)^3}\left[-4d^2(2\sigma^{(-2,2)}(\gamma)\sigma^{(0,0)}(\gamma) + 1) + 4d\left(2r + 4\sigma^{(-2,2)}(\gamma)\right.\right.\\ &\quad \times\sigma^{(0,0)}(\gamma)r + \sigma^{(0,0)}(\gamma)\left(-2\sigma^{(-2,2)}(\gamma)\sigma^{(0,0)}(\gamma)^2 + \sigma^{(0,0)}(\gamma) - 4\sigma^{(0,1)}(\gamma)\right)\Big)\\ &\quad - 4r^2(2\sigma^{(-2,2)}(\gamma)\sigma^{(0,0)}(\gamma) + 1) - 4r\sigma^{(0,0)}(\gamma)\left(\sigma^{(0,0)}(\gamma)(2\sigma^{(-2,2)}(\gamma)\sigma^{(0,0)}(\gamma)\right.\\ &\quad \left.+ 3) - 4\sigma^{(0,1)}(\gamma)\right) + \sigma^{(0,0)}(\gamma)^3\left(\sigma^{(0,0)}(\gamma)(3 - 2\sigma^{(-2,2)}(\gamma)\sigma^{(0,0)}(\gamma)) + 8(\sigma^{(0,1)}(\gamma)\right.\\ &\quad \left.\left.\left. + 2\sigma^{(0,2)}(\gamma))\right) + 8\sigma^{(1,0)}(\gamma)^2 - 8\sigma^{(2,0)}(\gamma)\sigma^{(0,0)}(\gamma)\right].\end{aligned}$$

Now, viewing all the IV expansion terms $\sigma^{(n_1,n_2)}$ with $n_2 = 0, 1$ computed from *the cases* $n_2 = 0$ and 1 as inputs, we now match expansion terms of (28) and (29) in order to solve the desired IV expansion terms $\sigma^{(n_1,2)}$: We solve equations $\bar{p}_2^{(l)} = \tilde{p}_2^{(l)}$ for $l = -1, 0, 1$ recursively to obtain the closed-form formulae of $\sigma^{(-2,2)}$, $\sigma^{(-1,2)}$, and $\sigma^{(0,2)}$. Straightforward computation yields $\sigma^{(-2,2)}(\gamma) \equiv 0$ while $\sigma^{(-1,2)}$ and $\sigma^{(0,2)}$ are nonzero; see their closed-form formulae documented in Example 4 of Section S.2. This contradicts $L_2 = -2$, and leads to $L_2 = -1$. Similarly, all higher order terms $\sigma^{(n_1,2)}$ can be obtained recursively by equating higher order expansion terms $\bar{p}_2^{(l)}$ and $\tilde{p}_2^{(l)}$.

An alternative approach for obtaining the IV expansion terms relies on the computation of mixed derivatives in (10): The IV $\Sigma'(\epsilon,k',\gamma) = \Sigma(\epsilon^2, k'\epsilon, \gamma)$ solves the equation

$$f(\epsilon, k', \Sigma'(\epsilon,k',\gamma)) = 0, \tag{30}$$

where the function f is defined in (13). Based on the verified differentiability of f and $\Sigma'(\epsilon,k',\gamma)$, we can construct the bivariate Taylor expansion (9), i.e.,

$$\Sigma'^{(K_1,K_2)}(\epsilon,k',\gamma) = \sum_{n_2'=0}^{K_2}\sum_{n_1'=0}^{K_1}\varphi^{(n_1',n_2')}(\gamma)\epsilon^{n_1'}(k')^{n_2'},$$

with

$$\varphi^{(n_1',n_2')}(\gamma) = \frac{1}{n_1'!n_2'!}\frac{\partial^{n_1'+n_2'}}{\partial\epsilon^{n_1'}\partial(k')^{n_2'}}\Sigma'(0,0,\gamma), \tag{31}$$

by computing the involved mixed derivatives in (31). Indeed, for each pair of n_1' and n_2', we differentiate with respect to ϵ and k' Eq. (30) n_1' times and n_2' times respectively, and then let $(\epsilon,k') = (0,0)$. We repeat this from small values of n_1' and n_2' up to $n_1' = K_1$ and $n_2' = K_2$ to construct a system of equations with unknowns as $\varphi^{(n_1',n_2')}(\gamma)$. Starting from relatively simple equations and progressing to more complicated ones, we can recursively solve all expansion terms $\varphi^{(n_1',n_2')}(\gamma)$. Finally, following the procedure described after Assumption 1, we obtain a bivariate expansion of $\Sigma(\tau,k,\gamma)$ with respect to ϵ and k by replacing k' with k/ϵ in (11) with $i = j = 0$. Routine computations show that the recovered bivariate expansion of $\Sigma(\tau,k,\gamma)$ with respect to ϵ and k coincides with what we have obtained directly following the order-matching procedure.

3.4. The general case

Following a procedure similar to that illustrated for the Merton (1976) model in the previous section, one can construct the expansion (11) of $\Sigma_{i,j}$ under the general SV model (2a)–(2b) with the lower bound $L_{n_2}^{(i,j)}$ given by $L_{n_2}^{(0,0)} = \min(0, 1-n_2)$ and $L_{n_2}^{(i,j)} = 1-n_2-2i-j$ when $i+j > 0$. All the expansion terms can be calculated in closed form. To avoid repetition, we summarize the results as Theorem S.1 in Section S.1.1. Additionally, we establish closed-form bivariate expansions, with respect to the time-to-maturity τ and log-moneyness k, of the option price and its sensitivity, which serve as an input for constructing the IV expansion as was the case in the previous section. The result is summarized as Proposition S.1 in Section S.1.2. To illustrate our IV expansion, we provide closed-form expansion formulae under six representative models in Section S.2.

From the dynamics (2a), the instantaneous SV $v_0(X_t)$ of the asset price is given by[13]

$$v_0(X_t) = \sqrt{v_1^2(X_t) + v_2^2(X_t) + \cdots + v_n^2(X_t)}, \tag{32}$$

which coincides with the leading expansion term $\sigma^{(0,0)}(X_t)$ in light of (S.5) in Theorem S.1. As a generalization of (15), by setting $i = j = k = J_2 = 0$ in the bivariate expansion (11), we obtain the following univariate expansion of the at-the-money IV $\Sigma(\tau, 0, X_t)$ with respect to the square root of time-to-maturity $\epsilon = \sqrt{\tau}$:

$$\Sigma^{(J_1,0)}(\tau, 0, X_t) = \sum_{n_1=0}^{J_1} \sigma^{(n_1,0)}(X_t)\epsilon^{n_1}, \tag{33}$$

where, in this and the subsequent univariate expansions, the order J_1 is required to be nonnegative, i.e., $J_1 \geq 0$, as imposed for our bivariate expansion. The Taylor nature of expansion (33) suggests that the at-the-money IV approaches $\sigma^{(0,0)}(X_t)$, which coincides with the instantaneous SV $v_0(X_t)$ given in (32), as the time-to-maturity τ shrinks to zero. This is in agreement with the results in Ledoit et al. (2002) for continuous SV models and Durrleman (2008) for SV models with finite variation jumps showing that the at-the-money IV approaches the instantaneous SV as time-to-maturity shrinks to zero. Beyond this compatibility, our bivariate expansion (11) completes this limiting behaviour by providing any desired higher order behaviour of the IV surface resulting from a given SV model with or without jumps.

Indeed, similar to (33), we construct the marginal expansion of the IV sensitivity $\Sigma_{i,j}(\tau, k, X_t)$ for $i + j > 0$ in the at-the-money direction by plugging $k = J_2 = 0$ into the bivariate expansion (11).[14] That is to obtain the univariate expansion of $\Sigma_{i,j}(\tau, 0, X_t)$ as

$$\Sigma_{i,j}^{(J_1,0)}(\tau, 0, X_t) = \sum_{n_1=1-2i-j}^{J_1} \sigma_{i,j}^{(n_1,0)}(X_t)\epsilon^{n_1}. \tag{34}$$

Generally, the univariate expansion of at-the-money IV sensitivity $\Sigma_{i,j}(\tau, 0, X_t)$ incorporates negative power(s) of ϵ and is thus in the Laurent sense, as long as its lowest order $1-2i-j$ satisfies $1-2i-j \leq -1$, i.e., $2i+j \geq 2$. In this case, the at-the-money sensitivity $\Sigma_{i,j}(\tau, 0, X_t)$ explodes to infinity, as the time-to-maturity τ, or equivalently, its square root ϵ, shrinks to zero. For such explosive Laurent expansion, following the standard convention, its behaviour around the singularity point $\epsilon = 0$ can be understood through that of the Taylor expansion of the time-scaled IV sensitivity $\epsilon^{2i+j-1}\Sigma_{i,j}^{(J_1,0)}(\tau, 0, X_t)$ around $\epsilon = 0$.

For example, as a generalization of (22), by letting $i = 0$ and $j = 1$ in (34), we obtain the marginal expansion of the at-the-money slope $\Sigma_{0,1}(\tau, 0, X_t)$ with respect to $\epsilon = \sqrt{\tau}$ as

$$\Sigma_{0,1}^{(J_1,0)}(\tau, 0, X_t) = \sum_{n_1=0}^{J_1} \sigma_{0,1}^{(n_1,0)}(X_t)\epsilon^{n_1}, \text{ with } \sigma_{0,1}^{(n_1,0)}(X_t) = \sigma^{(n_1,1)}(X_t), \tag{35}$$

according to the relation (S.4) in Theorem S.1. Similarly, we obtain the expansions of convexity $\Sigma_{0,2}(\tau, 0, X_t)$ and term-structure slope $\Sigma_{1,0}(\tau, 0, X_t)$ as

$$\Sigma_{0,2}^{(J_1,0)}(\tau, 0, X_t) = \sum_{n_1=-1}^{J_1} \sigma_{0,2}^{(n_1,0)}(X_t)\epsilon^{n_1}, \text{ with } \sigma_{0,2}^{(n_1,0)}(X_t) = 2\sigma^{(n_1,2)}(X_t), \tag{36}$$

---

[13] Eq. (2a) can be equivalently written as

$$\frac{dS_t}{S_{t-}} = (r - d - \lambda(X_t)\bar{\mu})dt + \sqrt{v_1^2(X_t) + v_2^2(X_t) + \cdots + v_n^2(X_t)}dW_t^S + (\exp(J_t) - 1)dN_t,$$

where W_t^S is a Brownian motion constructed by $dW_t^S = v(X_t)\,[v_1^2(X_t) + v_2^2(X_t) + \cdots + v_n^2(X_t)]^{-\frac{1}{2}}\,dW_t$.

[14] However, such marginal expansions cannot be constructed in the short-maturity direction by letting in $\epsilon \to 0$ because of the explosive nature of the expansion resulting from the possible inclusion of negative powers of ϵ.

and

$$\Sigma_{1,0}^{(J_1,0)}(\tau,0,X_t)=\sum_{n_1=-1}^{J_1}\sigma_{1,0}^{(n_1,0)}(X_t)\epsilon^{n_1},\ \text{with}\ \sigma_{1,0}^{(n_1,0)}(X_t)=\frac{1}{2}(n_1+2)\sigma^{(n_1+2,0)}(X_t), \tag{37}$$

respectively. The slope expansion (35) is in the Taylor sense with respect to ϵ for involving only nonnegative powers of ϵ. This explains why the at-the-money slope converges to a finite value as the time-to-maturity shrinks to zero (see, e.g., the discussions in Yan, 2011 under the model of Merton, 1976). Nevertheless, the term-structure slope expansion (37) and the convexity expansion (36) are both in the Laurent sense with respect to ϵ, involving negative powers of ϵ. This reveals the explosive nature of these two at-the-money shape characteristics under the general SV model with jumps (2a)–(2b) as the time-to-maturity shrinks to zero.

Since (33) and (35)–(36) correspond to observable shape characteristics of the IV surface, they permit an explicit understanding of the impact of various parameters or components of the SV model with jumps on the IV surface. We will illustrate this in Section 4.3.

4. Generic bivariate SV model with jumps: Explicit formulae for the IV

In this section, we apply the closed-form IV expansion to a generic bivariate SV model. We show in particular that the slope of the IV smile is determined by the volatility-of-volatility functions and the jump component of the model, and analyse the role that jumps play in the positive explosion of the log-moneyness convexity and term-structure IV slope as the-time-to-maturity shrinks to zero. Then, specializing further to a one-factor affine SV with jumps model, we analyse the impact of this model's parameters on the shape of the IV surface, thereby providing new results for an otherwise well understood model.

4.1. Expansion for a bivariate SV model with jumps

We consider a generic bivariate SV with jumps model driven by a two-dimensional Brownian motion W_t and a jump process N_t with stochastic jump intensity $\lambda(x)$, i.e., $m=1$ and $n=2$ under the general setup in Section 3. That is, we specialize the model to

$$\frac{dS_t}{S_{t-}}=(r-d-\lambda(V_t)\bar{\mu})dt+v_1(V_t)dW_{1t}+(\exp(J_t)-1)dN_t, \tag{38a}$$

$$dV_t=\mu(V_t)dt+\sigma_1(V_t)dW_{1t}+\sigma_2(V_t)dW_{2t}, \tag{38b}$$

where, comparing with the general model (2a)–(2b), we set $X_t=V_t$, $v(x)=(v_1(x),0)$, and $\sigma(x)=(\sigma_1(x),\sigma_2(x))$. Here, we assume that the volatility function $v_1(x)$ takes positive values. Besides, we further assume that the jump size J_t is normally distributed with mean μ_J and variance σ_J^2, so that the jump compensator $\bar{\mu}$ is explicitly calculated according to (3) as $\bar{\mu}=\exp(\mu_J+\sigma_J^2/2)-1$. This assumption is not necessary for the analysis, but simplifies the exposition and interpretation of the formulae that follow; otherwise the formulae involve generalized moments of the assumed jump size distribution.

This setup assumes a self-driven volatility variable V_t, i.e., the functions μ, σ_1, and σ_2 depend only on V_t, and nests all existing one-factor SV models with or without jumps in the literature. For example, specifying the risk-neutral parameter set to be $\{\kappa,\theta,\xi,\rho,\lambda_0,\lambda_1\}$, we obtain the one-factor affine SV with jumps model proposed in Bates (1996) (resp. Pan, 2002) by setting $v_1(x)=\sqrt{x}$, $\mu(x)=\kappa(\theta-x)$, $\sigma_1(x)=\xi\rho\sqrt{x}$, $\sigma_2(x)=\xi\sqrt{1-\rho^2}\sqrt{x}$, and $\lambda(x)=\lambda_0$ (resp. $\lambda(x)=\lambda_1 x$), the log-OU with jumps model proposed in Andersen et al. (2002) by setting $v_1(x)=e^x$, $\mu(x)=\kappa(\theta-x)$, $\sigma_1(x)=\xi\rho$, $\sigma_2(x)=\xi\sqrt{1-\rho^2}$, and $\lambda(x)=\lambda_0+\lambda_1 e^{2x}$. In particular, by letting $\lambda(x)\equiv 0$, these examples reduce to their continuous counterparts, i.e., the continuous square-root SV model in Heston (1993) and the continuous log-OU model in Scott (1987). More generally, the results in this section apply to all the one-factor SV models with or without jumps listed in Panel A of Table 3 and Panel A of Table 4.

By specializing the our expansion results for IV and its sensitivities under the general model (2a)–(2b) (see Theorem S.1), we obtain the $(1,2)$th order expansion of the IV Σ:

Corollary 1. *The SV model with jumps (38a)–(38b) admits the following $(1,2)$th order IV expansion:*

$$\Sigma^{(1,2)}(\tau,k,X_t)=\sigma^{(0,0)}(X_t)+\sigma^{(1,0)}(X_t)\epsilon+\sigma^{(0,1)}(X_t)k+\sigma^{(1,1)}(X_t)\epsilon k$$
$$+\sigma^{(-1,2)}(X_t)\epsilon^{-1}k^2+\sigma^{(0,2)}(X_t)k^2+\sigma^{(1,2)}(X_t)\epsilon k^2,$$

where $\sigma^{(0,0)}(x)=v_1(x)$ and

$$\sigma^{(1,0)}(x)=\sqrt{\frac{\pi}{2}}\lambda(x)(-\bar{\mu}+2(\bar{\mu}+1)\mathcal{N}(\mu_+)-2\mathcal{N}(\mu_-)), \tag{39a}$$

$$\sigma^{(0,1)}(x)=\frac{1}{v_1(x)}[\lambda(x)\bar{\mu}+\frac{1}{2}\sigma_1(x)v_1'(x)],\ \sigma^{(-1,2)}(x)=\frac{1}{2v_1(x)^2}\sigma^{(1,0)}(x), \tag{39b}$$

Table 3
Dynamics of various continuous SV models.

Model	Reference	Dynamics
Panel A: One-factor continuous SV models		
Hull–White	Hull and White (1987)	$dS_t/S_t = (r-d)dt + \sqrt{V_t}(\sqrt{1-\rho^2}dW_{1t} + \rho dW_{2t})$ $dV_t = \mu V_t + \xi V_t dW_{2t}$
GARCH-SV	Nelson (1990), Meddahi (2001) Christoffersen et al. (2010)	$dS_t/S_t = (r-d)dt + \sqrt{V_t}(\sqrt{1-\rho^2}dW_{1t} + \rho dW_{2t})$ $dV_t = \kappa(\theta - V_t)dt + \xi V_t dW_{2t}$
Stein–Stein	Stein and Stein (1991) Schöbel and Zhu (1999)	$dS_t/S_t = (r-d)dt + \sigma_t(\sqrt{1-\rho^2}dW_{1t} + \rho dW_{2t})$ $d\sigma_t = \kappa(\theta - \sigma_t)dt + \xi dW_{2t}$
Heston	Heston (1993)	$dS_t/S_t = (r-d)dt + \sqrt{V_t}(\sqrt{1-\rho^2}dW_{1t} + \rho dW_{2t})$ $dV_t = \kappa(\theta - V_t)dt + \xi\sqrt{V_t}dW_{2t}$
3/2	Christoffersen et al. (2010)	$dS_t/S_t = (r-d)dt + \sqrt{V_t}(\sqrt{1-\rho^2}dW_{1t} + \rho dW_{2t})$ $dV_t = \kappa(\theta - V_t)V_t dt + \xi V_t^{3/2}dW_{2t}$
log-OU	Scott (1987) Andersen et al. (2002)	$dS_t/S_t = (r-d)dt + \exp(U_t)(\sqrt{1-\rho^2}dW_{1t} + \rho dW_{2t})$ $dU_t = (a - bU_t)dt + \xi dW_{2t}$
Log-linear	Gallant et al. (1999) Chernov et al. (2003)	$dS_t/S_t = (r-d)dt + \exp(U_t)(\sqrt{1-\rho^2}dW_{1t} + \rho dW_{2t})$ $dU_t = (a - bU_t)dt + (\xi_0 + \xi_1 U_t)dW_{2t}$
CEV-SV	Jones (2003)	$dS_t/S_t = (r-d)dt + \sqrt{V_t}(\sqrt{1-\rho^2}dW_{1t} + \rho dW_{2t})$ $dV_t = \kappa(\theta - V_t)dt + \xi V_t^{\beta}dW_{2t}$
Panel B: Two-factor continuous SV models		
DMR-SQR	Duffie et al. (2000)	$dS_t/S_t = (r-d)dt + \sqrt{V_t}(\sqrt{1-\rho^2}dW_{1t} + \rho dW_{2t})$ $dV_t = \kappa(\bar{V}_t - V_t)dt + \xi\sqrt{V_t}dW_{2t}$ $d\bar{V}_t = \kappa_0(\theta_0 - \bar{V}_t)dt + \xi_0\sqrt{\bar{V}_t}dW_{3t}$
Double-log-linear	Gallant et al. (1999) Chernov et al. (2003)	$dS_t/S_t = (r-d)dt + \eta\exp(U_{1t} + U_{2t})$ $\times(\sqrt{1-\rho_1^2-\rho_2^2}dW_{1t} + \rho_1 dW_{2t} + \rho_2 dW_{3t})$ $dU_{1t} = -b_1 U_{1t}dt + (\xi_{10} + \xi_{11}U_{1t})dW_{2t}$ $dU_{2t} = -b_2 U_{2t}dt + (\xi_{20} + \xi_{21}U_{2t})dW_{3t}$
Double-SQR	Christoffersen et al. (2009)	$dS_t/S_t = (r-d)dt + \sqrt{V_{1t}}(\sqrt{1-\rho_1^2}dW_{1t} + \rho_1 dW_{2t})$ $+ \sqrt{V_{2t}}(\sqrt{1-\rho_2^2}dW_{3t} + \rho_2 dW_{4t})$ $dV_{1t} = \kappa_1(\theta_1 - V_{1t})dt + \xi_1\sqrt{V_{1t}}dW_{2t}$ $dV_{2t} = \kappa_2(\theta_2 - V_{2t})dt + \xi_2\sqrt{V_{2t}}dW_{4t}$

$$\sigma^{(1,1)}(x) = \frac{\sqrt{\pi}\lambda(x)}{2\sqrt{2}v_1(x)^2}[2(r-d)\bar{\mu} + 2(\bar{\mu}+1)\mathcal{N}(\mu_+)(2d - 2r - v_1(x)^2) + \bar{\mu}v_1(x)^2$$
$$+ 2v_1(x)^2 - 2\mathcal{N}(\mu_-)(2d - 2r + v_1(x)^2)], \tag{39c}$$

$$\sigma^{(0,2)}(x) = \frac{1}{12v_1(x)^3}[\sigma_1(x)^2(2v_1(x)v_1''(x) - 3v_1'(x)^2) + 2v_1(x)\sigma_1(x)v_1'(x)\sigma_1'(x)$$
$$+ 2\sigma_2(x)^2 v_1'(x)^2 - 3\pi\lambda(x)^2(\bar{\mu} - 2(\bar{\mu}+1)\mathcal{N}(\mu_+) + 2\mathcal{N}(\mu_-))^2$$
$$+ 6\lambda(x)(\bar{\mu}\left(2d - 2r - \sigma_1(x)v_1'(x)\right) - (\bar{\mu}+2)v_1(x)^2)]. \tag{39d}$$

Here, μ_- and μ_+ are defined in (19), i.e., $\mu_- = \mu_J/\sigma_J$ and $\mu_+ = \mu_J/\sigma_J + \sigma_J$. Furthermore, it follows from (11) that the $(1,1)$th order expansion of the slope $\Sigma_{0,1}$ is

$$\Sigma_{0,1}^{(1,1)}(\tau, k, X_t) = \sigma_{0,1}^{(0,0)}(X_t) + \sigma_{0,1}^{(1,0)}(X_t)\epsilon + \sigma_{0,1}^{(-1,1)}(X_t)\epsilon^{-1}k + \sigma_{0,1}^{(0,1)}(X_t)k + \sigma_{0,1}^{(1,1)}(X_t)\epsilon k,$$

where $\sigma_{0,1}^{(0,0)}(x) = \sigma^{(0,1)}(x)$, $\sigma_{0,1}^{(1,0)}(x) = \sigma^{(1,1)}(x)$, $\sigma_{0,1}^{(-1,1)}(x) = 2\sigma^{(-1,2)}(x)$, and $\sigma_{0,1}^{(0,1)}(x) = 2\sigma^{(0,2)}(x)$, respectively, and the expansion terms $\sigma^{(0,1)}$, $\sigma^{(1,1)}$, $\sigma^{(-1,2)}$, and $\sigma^{(0,2)}$ are given above in (39b), (39c), (39b), and (39d), respectively.

4.2. Slope, convexity, and term-structure slope of the IV

In this section, we compute the short-maturity behaviour of the slope, convexity, and term-structure slope of the IV surface under the generic bivariate SV with jumps model (38a)–(38b), using the corresponding closed-form expansions in (35), (36), and (37), respectively.

Table 4
Dynamics of various SV models with jumps.

Model	Reference	Dynamics
Panel A: One-factor SV models with jumps		
One-factor affine SV with jumps	Bates (1996), Pan (2002) Andersen et al. (2002)	$dS_t/S_{t-} = (r - d - (\lambda_0 + \lambda_1 V_t)\,\bar{\mu})dt + \sqrt{V_t}dW_{1t} + (\exp(J_t) - 1)dN_t$ $dV_t = \kappa(\theta - V_t)dt + \xi\sqrt{V_t}[\rho dW_{1t} + \sqrt{1-\rho^2}dW_{2t}]$
log-OU SV with jumps	Andersen et al. (2002)	$dS_t/S_{t-} = (r - d - (\lambda_0 + \lambda_1 \exp(2U_t))\bar{\mu})dt + \exp(U_t)dW_{1t} + (\exp(J_t) - 1)dN_t$ $dU_t = (a - bU_t)dt + \xi[\rho dW_{1t} + \sqrt{1-\rho^2}dW_{2t}]$
Panel B: Two-factor SV models with jumps		
Two-factor affine SV with jumps	Bates (2000)	$dS_t/S_{t-} = (r - d - (\lambda_0 + \lambda_1 V_{1t} + \lambda_2 V_{2t})\,\bar{\mu})dt + \sqrt{V_{1t}}(\sqrt{1-\rho_1^2}dW_{1t} + \rho_1 dW_{2t}) + \sqrt{V_{2t}}(\sqrt{1-\rho_2^2}dW_{3t} + \rho_2 dW_{4t}) + (\exp(J_t) - 1)dN_t$ $dV_{1t} = \kappa_1(\theta_1 - V_{1t})dt + \xi_1\sqrt{V_{1t}}dW_{2t}$ $dV_{2t} = \kappa_2(\theta_2 - V_{2t})dt + \xi_2\sqrt{V_{2t}}dW_{4t}$
DMR-SQR SV with jumps	Aït-Sahalia et al. (2019)	$dS_t/S_{t-} = (r - d - (\lambda_0 + \lambda_1 V_t)\,\bar{\mu})dt + \sqrt{(1-\rho^2)V_t}dW_{1t} + \rho\sqrt{V_t}dW_{2t} + (\exp(J_t) - 1)dN_t$ $dV_t = \kappa\left(\bar{V}_t - V_t\right)dt + \xi\sqrt{V_t}dW_{2t}$ $d\bar{V}_t = \kappa_0\left(\theta_0 - \bar{V}_t\right)dt + \xi_0\sqrt{\bar{V}_t}dW_{3t}$

Note: In all the SV models with jumps, the jump size J_t is normally distributed with mean μ_J and variance σ_J^2 and thus the jump compensator $\bar{\mu}$ is explicitly calculated as $\bar{\mu} = \exp(\mu_J + \sigma_J^2/2) - 1$.

First, given a short time-to-maturity τ, the slope Taylor expansion (35) implies the dominating effect of the leading term $\sigma_{0,1}^{(0,0)}$. Applying our general result of IV sensitivity expansion given in Theorem S.1, we have:

Corollary 2. *The leading term of the at-the-money slope of the IV surface in the log-moneyness dimension is given by*

$$\sigma_{0,1}^{(0,0)}(x) = \sigma^{(0,1)}(x) = \frac{1}{v_1(x)}[\lambda(x)\bar{\mu} + \frac{1}{2}\sigma_1(x)v_1'(x)]. \tag{40}$$

Thus, the expansion term $\sigma_{0,1}^{(0,0)}$ consists of four components: the spot volatility $v_1(x)$, the stochastic intensity $\lambda(x)$, the mean of price jump $\bar{\mu}$, and the multiplicative term $\sigma_1(x)v_1'(x)$. Indeed, the term $\sigma_1(x)v_1'(x)$ can be interpreted as follows: By Itô's lemma, the dynamics of the spot volatility $v_t = v_1(V_t)$ follows

$$dv_t = \alpha(V_t)dt + \gamma(V_t)dW_{1t} + \eta(V_t)dW_{2t},$$

where the drift function α and two volatility functions γ and η are given by

$$\alpha(x) = v_1'(x)\mu(x) + \frac{1}{2}v_1''(x)(\sigma_1(x)^2 + \sigma_2(x)^2),\ \ \gamma(x) = v_1'(x)\sigma_1(x),\ \text{ and } \eta(x) = v_1'(x)\sigma_2(x),$$

respectively. Thus $\sigma_1(x)v_1'(x)$ serves as the volatility function of the volatility v_t attached to the common Brownian innovation W_{1t} of the asset price S_t and its volatility factor V_t.

Empirically, for options on S&P 500 index, the at-the-money slope of an IV smile is usually negative. From (40), we see that to generate a negative slope, the mean of price jump $\bar{\mu}$ or the volatility function $\sigma_1(x)v_1'(x)$ or both have to be negative, owing to the positiveness of the spot volatility $v_1(x)$ and the stochastic intensity $\lambda(x)$. Consequently, a negative mean $\bar{\mu}$ implies that jumps in price are downward under the risk-neutral expectation, while a negative sign of $\sigma_1(x)v_1'(x)$ implies the presence of a continuous leverage effect, i.e., a negative correlation between the Brownian innovations to the price S_t and its volatility v_t. The continuous leverage effect $\rho(V_t)$ is defined by

$$\rho(V_t) = \frac{v_1'(V_t)\sigma_1(V_t)}{|v_1'(V_t)|\sqrt{\sigma_1(V_t)^2 + \sigma_2(V_t)^2}},$$

for a generic bivariate SV model with jumps (38a)–(38b). The negativeness of $\rho(V_t)$ is equivalent to that of the volatility function $\sigma_1(x)v_1'(x)$ and in turn is of the same sign as the contribution of the continuous part of the SV model to the slope of the IV surface: recall (40).

Second, in the presence of jumps, the Laurent nature of the convexity expansion (36) implies that the at-the-money convexity explodes to positive infinity as the time-to-maturity shrinks to zero. Indeed, according to (36), the at-the-money convexity is mainly determined by its leading term $\sigma_{0,2}^{(-1,0)}(x)\epsilon^{-1}$ as the time-to-maturity approaches to zero. Applying our general result of IV sensitivity expansion given in Theorem S.1, we have:

Corollary 3. *The leading term of the at-the-money convexity in the log-moneyness dimension of the IV surface is given by*

$$\sigma_{0,2}^{(-1,0)}(x) = 2\sigma^{(-1,2)}(x) = \frac{\lambda(x)I}{v_1(x)^2}, \text{ with } I = \sqrt{\frac{\pi}{2}}[1 - 2\mathcal{N}(\mu_-) + (\bar{\mu}+1)(2\mathcal{N}(\mu_+) - 1)]. \tag{41}$$

Then, the explosion to positive infinity of the at-the-money slope follows from the positiveness of the above expansion term $\sigma_{0,2}^{(-1,0)}(x)$, i.e., the positiveness of the constant I, which is proved immediately in what follows.

The positiveness of I, for any parameters μ_J and σ_J, follows from a case-by-case analysis depending on the relation between μ_J and σ_J. If $-\sigma_J^2/2 \leq \mu_J \leq 0$, it suffices to verify that $1 - 2\mathcal{N}(\mu_-) \geq 0$, $(\bar{\mu}+1)(2\mathcal{N}(\mu_+) - 1) \geq 0$, and the equalities of these two inequalities do not hold simultaneously. The first inequality $1 - 2\mathcal{N}(\mu_-) \geq 0$ follows from the fact that $\mu_- \leq 0$, which is an immediate consequence of the definition of μ_- given in (19), i.e., $\mu_- = \mu_J/\sigma_J$. The equality holds if and only if $\mu_J = 0$. Besides, the second inequality $(\bar{\mu}+1)(2\mathcal{N}(\mu_+) - 1) \geq 0$ follows from the fact that $\bar{\mu}+1 > 0$ and $2\mathcal{N}(\mu_+) - 1 > 0$, which are immediately guaranteed by the definition of $\bar{\mu}$ and μ_+ given in (3) and (19), i.e., $\bar{\mu} = \exp(\mu_J + \sigma_J^2/2) - 1$ and $\mu_+ = (\mu_J/\sigma_J) + \sigma_J$, respectively. The equality holds if and only if $\mu_J = -\sigma_J^2/2$. Otherwise, if $\mu_J > 0$ or $\mu_J < -\sigma_J^2/2$, the positiveness of I can be seen from the following alternative representation of (41):

$$I = \sqrt{\frac{\pi}{2}}(I_1 + I_2), \text{ with } I_1 = -\bar{\mu}(1 - 2\mathcal{N}(\mu_-)) \text{ and } I_2 = 2(\bar{\mu}+1)(\mathcal{N}(\mu_+) - \mathcal{N}(\mu_-)).$$

It suffices to show that $I_1 > 0$ and $I_2 > 0$ based on the aforementioned definitions of $\bar{\mu}$, μ_-, and μ_+. The first inequality $I_1 > 0$ follows from the fact that, if $\mu_J > 0$ (resp. $\mu_J < -\sigma_J^2/2$), we have $\bar{\mu} > 0$ (resp. $\bar{\mu} < 0$) as well as $\mu_- > 0$ (resp. $\mu_- < 0$) and thus $1 - 2\mathcal{N}(\mu_-) < 0$ (resp. $1 - 2\mathcal{N}(\mu_-) > 0$). The second inequality $I_2 > 0$ follows from the fact that $\bar{\mu}+1 > 0$ as well as $\mathcal{N}(\mu_+) - \mathcal{N}(\mu_-) > 0$, because of $\mu_+ > \mu_-$ owing to the positiveness of the parameter σ_J.

Third, with the presence of jumps, the term-structure slope also explodes to positive infinity as the time-to-maturity shrinking to zero, for the same reason as the at-the-money convexity. This follows from the Laurent nature of the term-structure slope expansion (37). The direction of such an explosion hinges on the sign of the leading term $\sigma_{1,0}^{(-1,0)}(x)$. Applying our general result of the IV sensitivity expansion given in Theorem S.1, we have:

Corollary 4. *The leading term of the at-the-money term-structure slope of the IV surface is given by*

$$\sigma_{1,0}^{(-1,0)}(x) = \frac{1}{2}\sigma^{(1,0)}(x) = \frac{\lambda(x)I}{2},$$

where the constant I is defined in (41).

The positiveness of constant I, as proved above, implies that of the expansion term $\sigma_{1,0}^{(-1,0)}(x)$.

4.3. Example: impact of the different parameters of a one-factor affine SV model with jumps on the IV

In this section, we study the impact on the shape of the IV surface of the different parameters of a one-factor affine SV model with jumps:

$$\frac{dS_t}{S_{t-}} = (r - d - (\lambda_0 + \lambda_1 V_t)\bar{\mu})dt + \sqrt{V_t}dW_{1t} + (\exp(J_t) - 1)dN_t,$$
$$dV_t = \kappa(\theta - V_t)dt + \xi\sqrt{V_t}[\rho dW_{1t} + \sqrt{1-\rho^2}dW_{2t}].$$

Here, W_{1t} and W_{2t} are two independent standard Brownian motions. The positive parameters κ, θ, and ξ describe the speed of mean-reversion, the long-run mean, and the volatility of variance process V_t, respectively. We assume that Feller's condition holds: $2\kappa\theta > \xi^2$. The leverage effect parameter $\rho \in [-1, 1]$ represents the instantaneous correlation between the Brownian innovations to the asset price and its variance. N_t is a Cox process with linear stochastic intensity $\lambda_0 + \lambda_1 V_t$ (Poisson when $\lambda_1 \equiv 0$), where the positive parameters λ_0 and λ_1 characterize the intercept and the slope of the intensity with respect to the variance V_t, respectively. The jump size J_t is assumed to be normally distributed with mean μ_J and variance σ_J^2, so that $\bar{\mu}$ is explicitly calculated according to (3) as $\bar{\mu} = \exp(\mu_J + \sigma_J^2/2) - 1$. This model follows from the generic bivariate SV model with jumps (38a)–(38b) by setting $v_1(x) = \sqrt{x}$, $\mu(x) = \kappa(\theta - x)$, $\sigma_1(x) = \rho\xi\sqrt{x}$, $\sigma_2(x) = \xi\sqrt{(1-\rho^2)x}$, and $\lambda(x) = \lambda_0 + \lambda_1 x$.

In what follows, we examine the impact of the spot variance v and parameters on the level, slope, convexity, and curvature along log-moneyness, as well as the term-structure slope, of the IV surface. The relevant expansions are given by (33) for the level, (35) and (36) for the slope and convexity along log-moneyness, respectively, and (37) for the slope along time-to-maturity. As to curvature, for an IV curve $\Sigma(\tau, k, v)$, viewed as a univariate function of log-moneyness k for a given time-to-maturity τ and state value v, curve geometry suggests the following definition of oriented curvature

$$(1 + (\Sigma_{0,1}(\tau, k, v))^2)^{-\frac{3}{2}}\Sigma_{0,2}(\tau, k, v), \tag{42}$$

which involves both log-moneyness slope $\Sigma_{0,1}$ and convexity $\Sigma_{0,2}$. The curvature is defined simply by the absolute value. With this definition, a curlier curve has a larger curvature rather than a greater convexity. Then, similar to the

constructions of expansions (33) and (35)–(36), performing a bivariate expansion of (42) with respect to ϵ and k, as well as evaluating it at $k = 0$, we compute the following Jth order expansion for evaluating the at-the-money oriented curvature:

$$\mathcal{U}^{(J)}(\tau, v) = \sum_{i=-1}^{J} u_i(v)\epsilon^i, \text{ with } u_{-1}(v) = 2(1+\sigma^{(0,1)}(v)^2)^{-\frac{3}{2}}\sigma^{(-1,2)}(v), \tag{43}$$

for any integer $J \geq 0$. All the aforementioned expansions can be explicitly determined by applying our general IV expansion result given in Theorem S.1:

$$\sigma^{(0,0)}(v) = \sqrt{v}, \ \sigma^{(1,0)}(v) = \sqrt{\frac{\pi}{2}}(\lambda_0 + \lambda_1 v)(-\bar{\mu} + 2(\bar{\mu}+1)\mathcal{N}(\mu_+) - 2\mathcal{N}(\mu_-)), \tag{44a}$$

$$\sigma^{(0,1)}(v) = \frac{1}{4\sqrt{v}}[4(\lambda_0 + \lambda_1 v)\bar{\mu} + \xi\rho], \ \sigma^{(-1,2)}(v) = \frac{1}{2v}\sigma^{(1,0)}(v), \tag{44b}$$

$$\begin{aligned}\sigma^{(2,0)}(v) = \frac{1}{96\sqrt{v}}[&24\theta\kappa + 48\lambda_0^2\bar{\mu}^2 - 12v(2\kappa + \lambda_0(-8\lambda_1\bar{\mu}^2 + 4\bar{\mu} + 8) + 2\lambda_1\bar{\mu}\xi\rho - \xi\rho) + \xi^2\rho^2 \\ &+ (d-r)(96(\lambda_0 + \lambda_1 v)\bar{\mu} + 24\xi\rho) + 24\lambda_0\bar{\mu}\xi\rho - 4\xi^2 + 48\lambda_1 v^2(\lambda_1\bar{\mu}^2 - \bar{\mu} - 2)],\end{aligned} \tag{44c}$$

where μ_- and μ_+ are defined in (19), i.e., $\mu_- = \mu_J/\sigma_J$ and $\mu_+ = (\mu_J/\sigma_J) + \sigma_J$.

Table 5 gives the closed-form expressions driving the impact of the different parameters of the model, with Panels from A to I concerning κ, θ, ξ, ρ, λ_0, λ_1, μ_J, σ_J, and the spot variance v, respectively. We illustrate in Figs. 7 and 8 the impact of these parameters on the IV surface under representative parameter values. We take the diffusion parameters κ and θ as well as the base jump intensity parameter λ_0 as examples, and investigate their impact on the one-month at-the-money level, slope, and term-structure slope of the IV surface. Each impact of parameter κ, θ, or λ_0 is summarized and analysed in the corresponding row of Panel A, Panel B, or Panel E, respectively. Consider the impact of these three parameters on the IV level as examples. Recall that the level is approximated by expansion (33) as exhibited in common in the second cells of the first rows from Panel A, Panel B, and Panel E, i.e.,

$$\Sigma^{(J,0)}(\tau, 0, v) = \sum_{l=0}^{J} \sigma^{(l,0)}(v)\epsilon^l.$$

For an arbitrary parameter, we naturally regard the lowest order term involving it as its most influential term, when $\epsilon = \sqrt{\tau}$ is sufficiently small. According to the closed-form formulae of expansion terms $\sigma^{(0,0)}$ and $\sigma^{(1,0)}$ given in (44a), as well as $\sigma^{(2,0)}$ given in (44b), we identify the most influential terms of the parameters κ, θ, and λ_0 as $\sigma^{(2,0)}$, $\sigma^{(2,0)}$, and $\sigma^{(1,0)}$, respectively.

For each of these parameters, we disentangle, in what follows, the source of impact based on the corresponding most influential term. First, as to the parameter κ, in its most influential term $\sigma^{(2,0)}$, the part depending on κ is $\kappa(\theta - v)/(4\sqrt{v})$, which is spelt out in the third cell of the first row from Panel A. As shown in the fourth cell on the same row, the impact of κ on the level is sensitive to different scenarios depending on the relation between the spot variance v and the long-run mean parameter θ of the variance process V_t. For example, if $v < \theta$, as κ increases, the level becomes higher. This is illustrated in the upper left panel of Fig. 7, which is numerically plotted. Second, as to the parameter θ, in its most influential term $\sigma^{(2,0)}$, the part depending on θ is $\kappa\theta/(4\sqrt{v})$. Owing to $\kappa, v > 0$, the level unconditionally becomes higher, as θ increases. This is reported in the first row of Panel B and is illustrated in the upper middle panel of Fig. 7. Third, as to the parameter λ_0, in its most influential term $\sigma^{(1,0)}$, the part depending on λ_0 is $\lambda_0 I$ with the constant I defined in (41). Since I is positive for any parameters μ_J and σ_J, as proved in Section 4.2, the level unconditionally becomes higher, as λ_0 increases. This is documented in the first row of Panel E and is illustrated in the central panel of Fig. 7.

Moreover, corresponding to the second (resp. third) row of Panel A, Panel B, or Panel E in Table 5, a similar procedure proceeds for disentangling the source of impact on the slope (resp. term-structure slope) of the parameter κ, θ, or λ_0, respectively. Clearly, as illustrated above, this type of dependence is not trivial and not easy to guess (or even assess numerically) in the absence of these closed-form expressions.

Are the impact of jump parameters or those of the diffusion parameters more dominating for short-maturity at-the-money IV shape characteristics? We notice that, on level, convexity, and term-structure slope, the impact of all the jump parameters λ_0, λ_1, μ_J, and σ_J are more dominating than those of the diffusion parameters κ and θ, when the time-to-maturity is sufficiently small. Taking the level for instance, this is simply because the most influential term for the former (resp. the latter) group of parameters is the first order term $\sigma^{(1,0)}$ in (44a) (resp. the second order term $\sigma^{(2,0)}$ in (44c)) of the level expansion (33). Besides, taking the convexity as another example, the most influential term for the jump parameters is the leading term $\sigma_{0,2}^{(-1,0)}$ of the expansion (36), i.e., $2\sigma^{(-1,2)}$ according to (36). According to the closed-form expression of $\sigma^{(-1,2)}$ in (44b), it is obvious that $\sigma_{0,2}^{(-1,0)}$ solely depends on the jump parameters but not any diffusion parameters, and thus exhibits the dominating role of the jump parameters.

However, as to the impact on the slope, the jump parameters λ_0, λ_1, μ_J, and σ_J as well as the diffusion parameters ξ and ρ are equally contributive, since they simultaneously get involved in the leading term $\sigma_{0,1}^{(0,0)}$ of the slope expansion

Table 5
One-factor affine SV model with jumps: Impact of different parameters on the IV surface.

Panel A: Impact of parameter κ

Shape characteristic	Expansion	Most influential part involving κ	Impact as κ increases	Example figure
Level	(33)	$\kappa(\theta-v)/(4\sqrt{v})$ in $\sigma^{(2,0)}$	higher if $v<\theta$ invariant if $v=\theta$ lower if $v>\theta$	upper left panel of Fig. 7
Slope	(35)	$\kappa I_\kappa/(48v^{3/2})$ in $\sigma_{0,1}^{(2,0)}$, with I_κ in (T.1)	clockwise rotating if $I_\kappa<0$ invariant if $I_\kappa=0$ anti-clockwise rotating if $I_\kappa>0$	upper left panel of Fig. 7
Term-structure slope	(37)	$\kappa(\theta-v)/(4\sqrt{v})$ in $\sigma_{1,0}^{(0,0)}$	anti-clockwise rotating if $v<\theta$ invariant if $v=\theta$ clockwise rotating if $v>\theta$	upper left panel of Fig. 8

Panel B: Impact of parameter θ

Shape characteristic	Expansion	Most influential part involving θ	Impact as θ increases	Example figure
Level	(33)	$\kappa\theta/(4\sqrt{v})$ in $\sigma^{(2,0)}$	higher	upper middle panel of Fig. 7
Slope	(35)	$-\kappa\theta I_\theta/(48v^{3/2})$ in $\sigma_{0,1}^{(2,0)}$ with I_θ in (T.2)	anti-clockwise rotating if $I_\theta<0$ invariant if $I_\theta=0$ clockwise rotating if $I_\theta>0$	upper middle panel of Fig. 7
Term-structure slope	(37)	$\kappa\theta/(4\sqrt{v})$ in $\sigma_{1,0}^{(0,0)}$	anti-clockwise rotating	upper middle panel of Fig. 8

Panel C: Impact of parameter ξ

Shape characteristic	Expansion	Most influential part involving ξ	Impact as ξ increases	Example figure
Slope	(35)	$\rho\xi/(4\sqrt{v})$ in $\sigma_{0,1}^{(0,0)}$	downward steeper if $\rho<0$ invariant if $\rho=0$ upward steeper if $\rho>0$	upper right panel of Fig. 7
Curvature	(43)	$(4(\lambda_0+\lambda_1 v)\bar{\mu}+\xi\rho)^2$ in u_{-1}	upward curlier if $\bar{\mu}\rho>0$, or $\bar{\mu}=0$, or $\bar{\mu}\rho<0$ and $\xi>\lvert 4(\lambda_0+\lambda_1 v)\bar{\mu}/\rho\rvert$ invariant if $\rho=0$ upward flatter if if $\bar{\mu}\rho<0$ and $\xi<\lvert 4(\lambda_0+\lambda_1 v)\bar{\mu}/\rho\rvert$	upper right panel of Fig. 7

Panel D: Impact of parameter ρ

Shape characteristic	Expansion	Most influential part involving ρ	Impact as ρ increases	Example figure
Slope	(35)	$\rho\xi/(4\sqrt{v})$ in $\sigma_{0,1}^{(0,0)}$	anti-clockwise rotating	middle left panel of Fig. 7
Convexity	(36)	$-I_\rho/(24v^{3/2})$ in $\sigma_{0,2}^{(0,0)}$ with I_ρ in (T.3)	more concave or less convex if $\rho<6(\lambda_0+\lambda_1 v)\bar{\mu}/(5\xi)$ less concave or more convex if $\rho>6(\lambda_0+\lambda_1 v)\bar{\mu}/(5\xi)$	middle left panel of Fig. 7

Panel E: Impact of parameter λ_0

Shape characteristic	Expansion	Most influential part involving λ_0	Impact as λ_0 increases	Example figure
Level	(33)	$I\lambda_0$ in $\sigma^{(1,0)}$ with I in (41)	higher	central panel of Fig. 7
Slope	(35)	$\bar{\mu}/\sqrt{v}\lambda_0$ in $\sigma_{0,1}^{(0,0)}$	anti-clockwise rotating if $\bar{\mu}>0$ invariant if $\bar{\mu}=0$ clockwise rotating if $\bar{\mu}<0$	central panel of Fig. 7
Term-structure slope	(37)	$\bar{\mu}\lambda_0/(2\sqrt{v})$ in $\sigma_{1,0}^{(-1,0)}$	anti-clockwise rotating	central panel of Fig. 8

(*continued on next page*)

(35), and thus they enjoy the same most influential term. Indeed, according to the closed-form expression of $\sigma^{(0,1)}$ in (44b) as well as the relation between terms $\sigma^{(0,1)}$ and $\sigma_{0,1}^{(0,0)}$ in (35), the term $\sigma_{0,1}^{(0,0)}$ is given by

$$\sigma_{0,1}^{(0,0)}(v)=\sigma^{(0,1)}(v)=\frac{\xi\rho}{4\sqrt{v}}+\frac{1}{\sqrt{v}}(\lambda_0+\lambda_1 v)\bar{\mu}, \tag{45}$$

Table 5 (*continued*).

Panel F: Impact of parameter λ_1

Shape characteristic	Expansion	Most influential part involving λ_1	Impact as λ_1 increases	Example figure
Level	(33)	$vI\lambda_1$ in $\sigma^{(1,0)}$ with I in (41)	higher	middle right panel of Fig. 7
Slope	(35)	$\bar{\mu}\sqrt{v}\lambda_1$ in $\sigma_{0,1}^{(0,0)}$	anti-clockwise rotating if $\bar{\mu} > 0$ invariant if $\bar{\mu} = 0$ clockwise rotating if $\bar{\mu} < 0$	middle right panel of Fig. 7

Panel G: Impact of parameter μ_J

Shape characteristic	Expansion	Most influential part involving μ_J	Impact as μ_J increases	Example figure
Level	(33)	$(\lambda_0 + \lambda_1 v)I$ in $\sigma^{(1,0)}$ with I in (41)	higher if $\mu_J > -\sigma_J^2$ invariant if $\mu_J = -\sigma_J^2$ lower if $\mu_J < -\sigma_J^2$	lower left panel of Fig. 7
Slope	(35)	$(\lambda_0 + \lambda_1 v)\bar{\mu}/\sqrt{v}$ in $\sigma_{0,1}^{(0,0)}$	anti-clockwise rotating	lower left panel of Fig. 7
Term-structure slope	(37)	$(\lambda_0 + \lambda_1 v)I/2$ in $\sigma_{1,0}^{(-1,0)}$ with I in (41)	anti-clockwise rotating if $\mu_J > -\sigma_J^2$ invariant if $\mu_J = -\sigma_J^2$ clockwise rotating if $\mu_J < -\sigma_J^2$	lower left panel of Fig. 8

Panel H: Impact of parameter σ_J

Shape characteristic	Expansion	Most influential part involving σ_J	Impact as σ_J increases	Example figure
Level	(33)	$(\lambda_0 + \lambda_1 v)I$ in $\sigma^{(1,0)}$ with I in (41)	higher if $I_\sigma^{(1)} < 0$ invariant if $I_\sigma^{(1)} = 0$ lower if $I_\sigma^{(1)} > 0$ with $I_\sigma^{(1)}$ given in (T.4)	lower middle panel of Fig. 7
Curvature	(43)	$I_\sigma^{(2)}$ in u_{-1} with $I_\sigma^{(2)}$ in (T.5)	upward curlier if $\partial I_\sigma^{(2)}/\partial\sigma_J > 0$ invariant if $\partial I_\sigma^{(2)}/\partial\sigma_J = 0$ upward flatter if $\partial I_\sigma^{(2)}/\partial\sigma_J < 0$	lower middle panel of Fig. 7
Term-structure slope	(37)	$(\lambda_0 + \lambda_1 v)I/2$ in $\sigma_{1,0}^{(-1,0)}$ with I in (41)	anti-clockwise rotating if $I_\sigma^{(1)} < 0$ invariant if $I_\sigma^{(1)} = 0$ clockwise rotating if $I_\sigma^{(1)} > 0$ with $I_\sigma^{(1)}$ given in (T.4)	lower middle panel of Fig. 8

Panel I: Impact of parameter v (spot variance)

Shape characteristic	Expansion	Most influential part involving v	Impact as v increases	Example figure
Level	(33)	$\sqrt{v}$ in $\sigma^{(0,0)}$	higher	lower right panel of Fig. 7
Slope	(35)	$\sigma_{0,1}^{(0,0)}$ given in (45)	anti-clockwise rotating if $4\bar{\mu}(\lambda_1 v - \lambda_0) - \xi\rho > 0$ invariant if $4\bar{\mu}(\lambda_1 v - \lambda_0) = \xi\rho$ clockwise rotating if $4\bar{\mu}(\lambda_1 v - \lambda_0) - \xi\rho < 0$	lower right panel of Fig. 7

Notations:

$I_\kappa = 12(v-\theta)(\lambda_0 - \lambda_1 v)\bar{\mu} + (v - 5\theta)\xi\rho$ (T.1)

$I_\theta = 12(\lambda_0 - \lambda_1 v)\bar{\mu} + 5\xi\rho$ (T.2)

$I_\rho = \xi\rho(12(\lambda_0 + \lambda_1 v)\bar{\mu} + 5\xi\rho)$ (T.3)

$I_\sigma^{(1)} = \sigma_J(1 - 2\mathcal{N}(\mu_+)) - \sqrt{2/\pi}\exp(-\mu_+^2/2)$, with $\mu_+ = (\mu_J/\sigma_J) + \sigma_J$ (T.4)

$I_\sigma^{(2)} = \sqrt{2/\pi}I_\lambda/(16v + (4(\lambda_0 + \lambda_1 v)\bar{\mu} + \xi\rho)^2)^{3/2}$ (T.5)

Note: All the IV shape characteristics are at-the-money with time-to-maturity equal to one month.

with the mean jump size $\bar{\mu}$ explicitly given by $\exp(\mu_J + \sigma_J^2/2) - 1$. As the leading term of slope expansion (35), the term $\sigma_{0,1}^{(0,0)}$ in (45) serves as an accurate approximation for the short-maturity at-the-money slope. According to (45), the diffusion component $\xi\rho/(4\sqrt{v})$ and the jump component $(\lambda_0 + \lambda_1 v)\bar{\mu}/\sqrt{v}$ simultaneously affect the slope, which is expected to be downward in shape and negative in value. In fact, the volatility of variance parameter ξ takes positive values; the jump intensity parameters λ_0 and λ_1 both take positive values in order to reflect the base level and the volatility excitation of the intensity, respectively. Consequently, the negative slope (i.e., the downward steep shape) becomes more (resp. less) pronounced, as the leverage effect parameter ρ becomes more (resp. less) negative towards -1 or/and the mean jump size $\bar{\mu}$ becomes more (resp. less) negative. We note that the mean $\bar{\mu}$ measures the average size of jumps. Recalling definition (3), if $\bar{\mu}$ is negative (resp. positive), then the jumps are downward (resp. upward) on average.

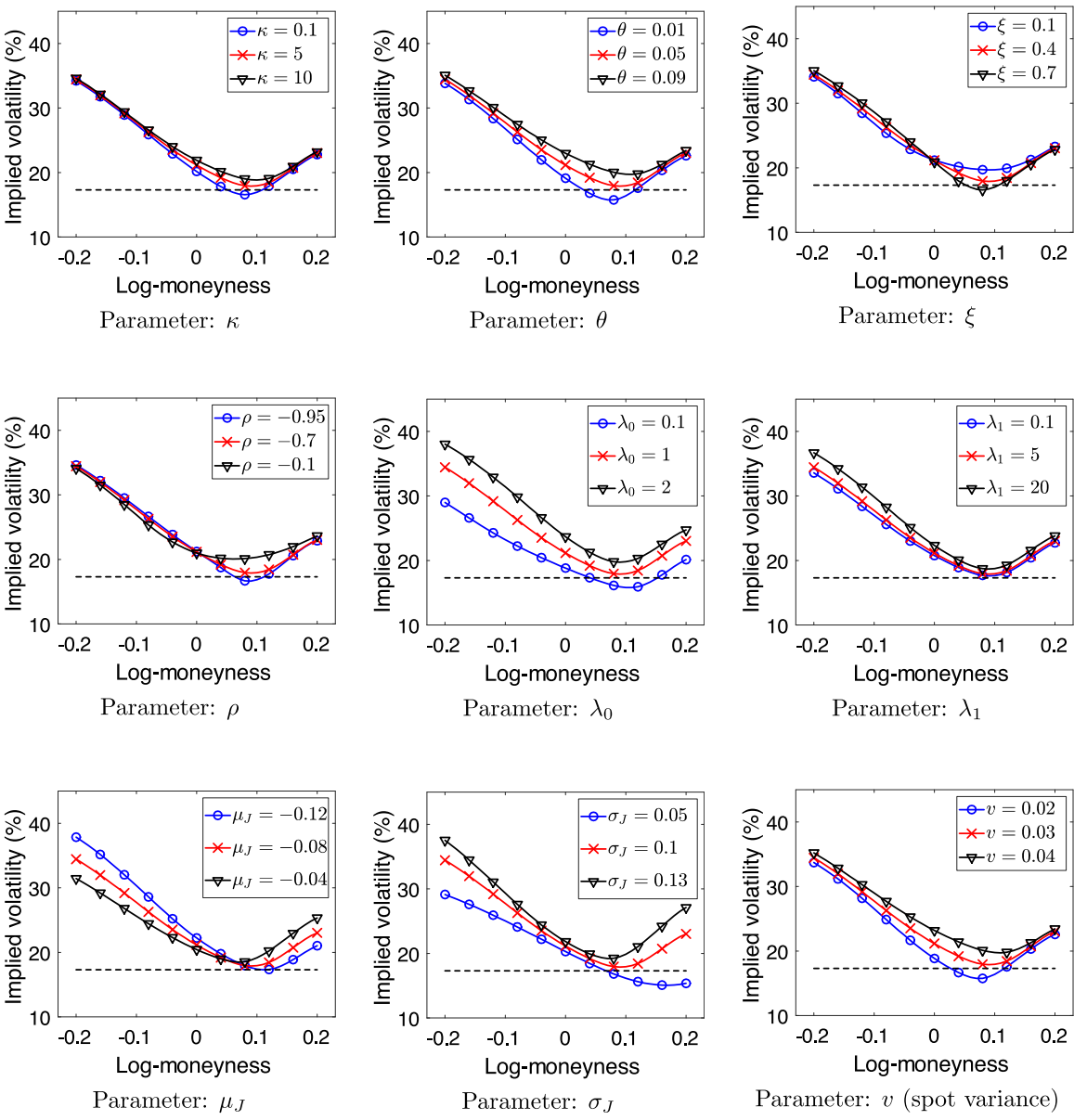

Fig. 7. One-month IV curves under the one-factor affine SV model with jumps. Note: In each panel, we plot three one-month IV curves along the log-moneyness under three parameter sets, respectively. All the IV curves with cross markers are plotted under the following benchmark parameter set: $\kappa = 5$, $\theta = 0.05$, $\xi = 0.4$, $\rho = -0.7$, $\lambda_0 = 1$, $\lambda_1 = 5$, $\mu_J = -0.08$, $\sigma_J = 0.1$, $r = 0.03$, $d = 0$, $s = 100$ and $v = 0.03$. Dashed lines indicate the level of the spot volatility $\sqrt{v} = 0.173$, which approximates the IV of at-the-money options with short time-to-maturity. In each panel, the curves with circle and triangle markers are plotted under two parameter sets obtained by perturbing only one parameter to two alternative values as reported in the legend of the panel and keeping all other parameters invariant, respectively.

In the S&P 500 index options market, empirical evidences lead to negative estimates of the leverage effect parameter ρ and the mean jump size $\bar{\mu}$ — both steepen the downward slope, see, e.g., the estimation results in Bakshi et al. (1997) and Pan (2002) among others. The impacts of parameters λ_0, λ_1, μ_J, σ_J, ξ, and ρ on the slope all hinge on (45) as their most influential term. We document the detailed analyses in Table 5.

Letting the jump components be zero reverts to the Heston model without jumps, and the term $\sigma_{0,1}^{(0,0)}$ in (45) degenerates to $\sigma_{0,1}^{(0,0)}(v) = \xi\rho/(4\sqrt{v})$. This formula reveals the impact of the constant leverage effect parameter ρ as well as the volatility of variance parameter ξ on the slope, which was noted in the literature for the Heston model, see, e.g., Chapter 3 of Gatheral (2006), and can be obtained via the expansion formula of Medvedev and Scaillet (2007); see

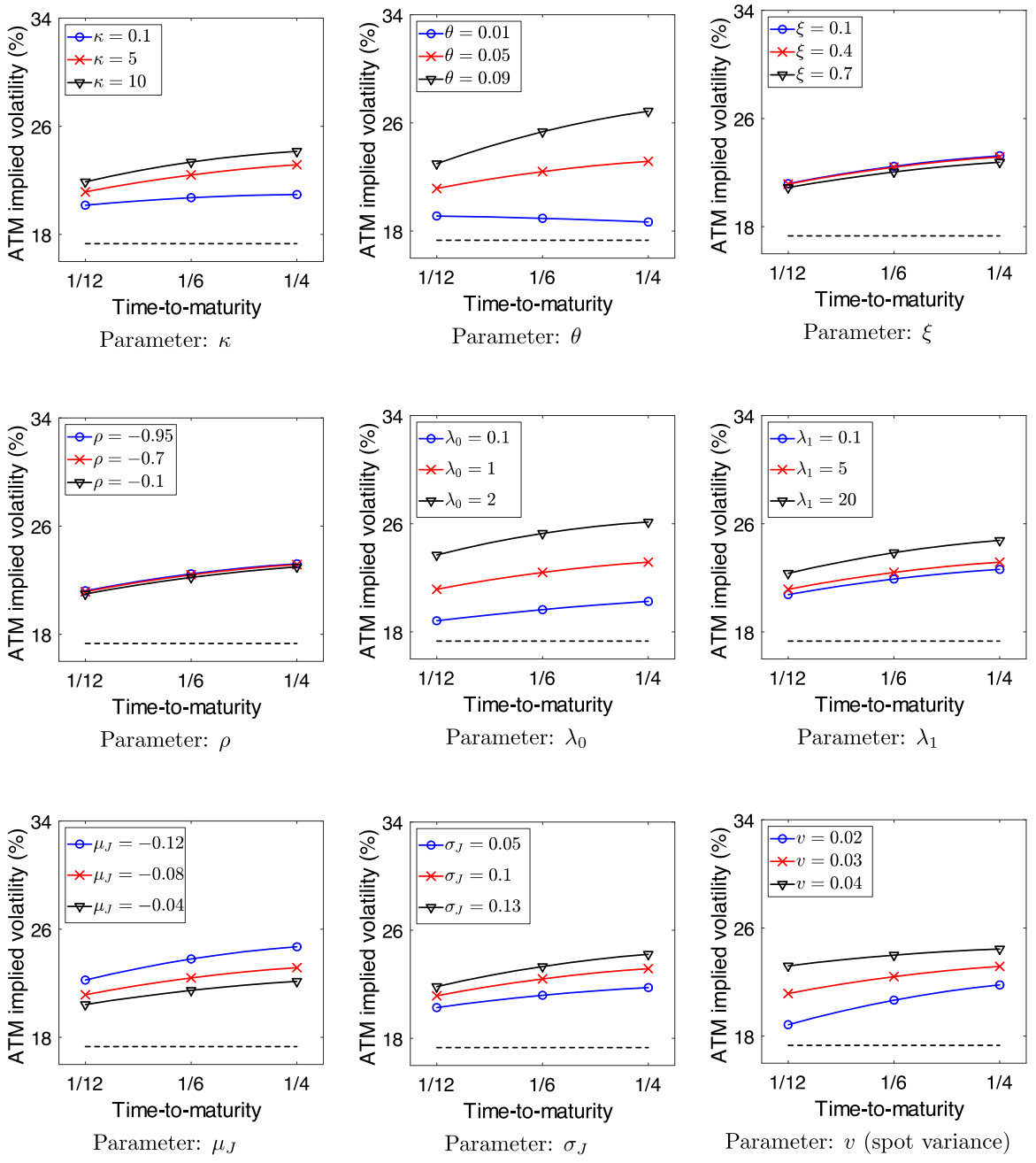

Fig. 8. At-the-money term-structure IV curves under the one-factor affine SV model with jumps. Note: In each panel, we plot three at-the-money term-structure IV curves along the time-to-maturity, under the same parameter sets employed in the corresponding panel of Fig. 7. All the dash lines indicate the level of the spot volatility $\sqrt{v} = 0.173$, which approximates the IV of at-the-money options with extremely short time-to-maturity (see discussions in Durrleman, 2008).

also Ledoit et al. (2002) for the impact of v on level. Another special case arises by letting the SV components be zero, i.e., $\kappa = \theta = \xi = \rho = 0$, and letting $\lambda_1 = 0$. This leads to the model of Merton (1976) with a constant volatility equal to $\sqrt{v_0}$. The term $\sigma_{0,1}^{(0,0)}$ in (45) degenerates to $\sigma_{0,1}^{(0,0)}(v_0) = \lambda_0\bar{\mu}/\sqrt{v_0}$. This formula shows not only the impact of the intensity parameter λ_0 and the mean jump size $\bar{\mu}$ on the slope under the model of Merton (1976) but also the limit of at-the-money slope as the time-to-maturity τ approaches to zero, owing to the Taylor nature of the slope expansion (35), which were noted in Proposition 2 of Yan (2011). These specific at-the-money leading term effects are generalized by our high order expansions under the generic SV model with jumps.

Table 6
Closed-form formulae for at-the-money level, slope, and convexity expansions for the continuous SV models listed in Table 3.

Model	Expansions of the model-version level, slope, and convexity		
	Level: $\Sigma^{(0,0)}$	Slope: $\Sigma^{(0,0)}_{0,1}$	Convexity: $\Sigma^{(0,0)}_{0,2}$
Panel A: One-factor continuous SV models			
Hull–White	$\sqrt{v}$	$\xi\rho/4$	$\xi^2(2-3\rho^2)/(24\sqrt{v})$
GARCH-SV	$\sqrt{v}$	$\xi\rho/4$	$\xi^2(2-3\rho^2)/(24\sqrt{v})$
Stein–Stein	σ	$\xi\rho/(2\sigma)$	$\xi^2(2-5\rho^2)/(6\sigma^3)$
Heston	$\sqrt{v}$	$\xi\rho/(4\sqrt{v})$	$\xi^2(2-5\rho^2)/(24v^{3/2})$
3/2	$\sqrt{v}$	$\xi\rho\sqrt{v}/4$	$\xi^2(2-\rho^2)\sqrt{v}/24$
Log-OU	e^u	$\xi\rho/2$	$\xi^2(2-3\rho^2)/(6e^u)$
Log-linear	e^u	$(\xi_0+\xi_1 u)\rho/2$	$[(2-3\rho^2)(\xi_0+\xi_1 u)^2 + 2\rho^2\xi_1(\xi_0+\xi_1 u)]/(6e^u)$
CEV-SV	$\sqrt{v}$	$\xi\rho v^{\beta-1}/4$	$\xi^2(2-(7-4\beta)\rho^2)v^{2\beta-5/2}/24$
Panel B: Two-factor continuous SV models			
DMR-SQR	$\sqrt{v}$	$\xi\rho/(4\sqrt{v})$	$\xi^2(2-5\rho^2)/(24v^{3/2})$
Double log-linear	$\eta e^{u_1+u_2}$	$[(\xi_{10}+\xi_{11}u_1)\rho_1 + (\xi_{20}+\xi_{21}u_2)\rho_2]/2$	$[((\xi_{10}+\xi_{11}u_1)^2+\xi_{11}\rho_1^2(\xi_{10}+\xi_{11}u_1)+(\xi_{20}+\xi_{21}u_2)^2+\xi_{21}\rho_2^2(\xi_{20}+\xi_{21}u_2))/3-(\rho_1\times(\xi_{10}+\xi_{11}u_1)+\rho_2(\xi_{20}+\xi_{21}u_2))^2/2]/(\eta e^{u_1+u_2})$
Double-SQR	$\sqrt{v_1+v_2}$	$(v_1\xi_1\rho_1+v_2\xi_2\rho_2)/(4(v_1+v_2)^{3/2})$	$[v_1^2\xi_1^2(2-5\rho_1^2)+v_2^2\xi_2^2(2-5\rho_2^2)+2v_1v_2(\xi_1^2(2\rho_1^2+1)+\xi_2^2\times(2\rho_2^2+1)-9\xi_1\xi_2\rho_1\rho_2)]/(24(v_1+v_2)^{7/2})$

5. Which SV models fit the IV data?

We now turn to the question of which SV model(s), with or without jumps, are capable of generating IV surfaces with shape characteristics that match the stylized facts outlined in Section 2. We consider all the models listed in Tables 3 and 4, first the one-factor continuous SV models listed in Panel A of Table 3, then the multifactor ones listed in Panel B of Table 3, and finally the one-factor and two-factor SV with jumps models listed in Table 4. This analysis identifies the respective roles of both the continuous and the jump components in terms of matching the empirical properties of the IV surface as outlined in Section 2.

Corresponding to the market versions of the shape characteristics listed in Table 2, the model versions of level, slope, convexity, and the term-structure slope can be approximated by expansions (33), (35), (36), and (37), respectively. To conduct comparative analysis, we will employ the zeroth order cases of these expansions which are given by

$$\Sigma^{(0,0)}(\tau,0,x)=\sigma^{(0,0)}(x),\ \ \Sigma^{(0,0)}_{0,1}(\tau,0,x)=\sigma^{(0,0)}_{0,1}(x), \tag{46}$$

$$\Sigma^{(0,0)}_{0,2}(\tau,0,x)=\sigma^{(-1,0)}_{0,2}(x)\epsilon^{-1}+\sigma^{(0,0)}_{0,2}(x), \tag{47}$$

$$\Sigma^{(0,0)}_{1,0}(\tau,0,x)=\sigma^{(-1,0)}_{1,0}(x)\epsilon^{-1}+\sigma^{(0,0)}_{1,0}(x), \tag{48}$$

respectively, with $\epsilon=\sqrt{\tau}$. Except for $\sigma^{(0,0)}$, each expansion term appearing in (46)–(48) coincides with a high order expansion term $\sigma^{(n_1,n_2)}$ of IV expansion (11) for $i=j=0$ up to some constant, e.g., $\sigma^{(0,0)}_{0,1}(x)=\sigma^{(0,1)}(x)$ and $\sigma^{(-1,0)}_{0,2}(x)=2\sigma^{(-1,2)}(x)$, among others. In the rest of this section, we abbreviate the expansions $\Sigma^{(0,0)}(\tau,0,x)$, $\Sigma^{(0,0)}_{0,1}(\tau,0,x)$, $\Sigma^{(0,0)}_{0,2}(\tau,0,x)$, and $\Sigma^{(0,0)}_{1,0}(\tau,0,x)$ to $\Sigma^{(0,0)}$, $\Sigma^{(0,0)}_{0,1}$, $\Sigma^{(0,0)}_{0,2}$, and $\Sigma^{(0,0)}_{1,0}$, respectively, unless otherwise indicated.

5.1. Choosing a continuous one-factor SV model

Under continuous SV models considered in Table 3, i.e., model (2a)–(2b) without jumps, the expansions can be obtained by simply setting all the jump components be zero in the corresponding ones calculated according to our general result in Theorem S.1 under the SV model with jumps. Table 6 reports the closed-form formulae for $\Sigma^{(0,0)}$, $\Sigma^{(0,0)}_{0,1}$, and $\Sigma^{(0,0)}_{0,2}$, for all the continuous SV models listed in Table 3.

We begin by discussing how one-factor models fit *Stylized fact 1* in terms of the sign of level-slope correlation, based on the expansions $\Sigma^{(0,0)}$ and $\Sigma^{(0,0)}_{0,1}$ of the level and slope. Without loss of generality, we assume the leverage effect parameter

ρ to be negative for all the models. The Stein–Stein model, the Heston model, the log-linear model with $\xi_1 < 0$, and the CEV-SV model with $\beta < 1$ all imply positive correlations, and thus reconcile *Stylized fact 1* for the year 2016 as shown in the lower left panel of Fig. 2. Likewise, the 3/2 model, the log-linear model with $\xi_1 > 0$, and the CEV-SV model with $\beta > 1$ all imply negative correlations, and thus reconcile *Stylized fact 1* for the year of 2010 as shown in the upper right panel of Fig. 2. Indeed, for example, the dependence between $\Sigma^{(0,0)}$ and $\Sigma^{(0,0)}_{0,1}$ under the Heston model can be seen from the slope expansion

$$\Sigma^{(0,0)}_{0,1}(\tau, 0, v) = \frac{\xi\rho}{4\sqrt{v}}, \tag{49}$$

which is usually negative due to the sign of the leverage effect parameter ρ. Thus, the slope becomes larger in value and flatter in shape, as the level expansion $\Sigma^{(0,0)}(\tau, 0, v) = \sqrt{v}$ increases. Besides, for the log-linear model with $\xi_1 = 0$ and the CEV-SV model with $\beta = 1$, we find that their level expansion $\Sigma^{(0,0)}$ and slope expansion $\Sigma^{(0,0)}_{0,1}$ are uncorrelated. We note that the log-linear model with $\xi_1 = 0$ reduces to the log-OU model and the CEV-SV model with $\beta = 1$ reduces to the GARCH-SV model. Thus, the log-OU and GARCH-SV model fit *Stylized fact 1* for the year 2017.

As discussed above, suitable one-factor models can be selected to produce the desired sign of correlation between level and slope. A common limitation among all of them is their lack of flexibility in reproducing sufficient variation of the data as shown in Fig. 2. More precisely, under all the one-factor models considered here, the slope $\Sigma^{(0,0)}_{0,1}$ is either a constant or fully determined by the level $\Sigma^{(0,0)}$. Consider the Heston model as an example. Given a realization of level $\Sigma^{(0,0)}(\tau, 0, v) = \sqrt{v}$, the slope $\Sigma^{(0,0)}_{0,1}$ is totally determined as $\xi\rho/(4\sqrt{v})$ according to (49). We will discuss how adding a second volatility factor to the SV model relaxes this limitation in Section 5.2.

To match *Stylized fact 2*, the expansion $\Sigma^{(0,0)}_{0,2}$ of convexity needs to be able to flexibly generate both positive and negative values under different parameter sets. The relevant formulae are given in Table 6. We see there that the 3/2 model and the CEV-SV model for $\beta \geq 5/4$, cannot produce negative values, since the correlation parameter ρ is between -1 and 1. Although failing to produce negative convexities, these two models can still be possibly employed to match *Stylized fact 2* in the period of 2009–2013, in which negative convexities are seldom observed, as shown in the left panel of Fig. 3. Among the models capable of generating both positive and negative local convexities, a common feature is that the negative local convexity can be produced by strong leverage effects induced by the Brownian innovations to price and its volatility, i.e., high absolute values of parameter ρ, which are often found when estimating these models (see, e.g., Jones, 2003 and Aït-Sahalia and Kimmel, 2007).

Stylized fact 3 (regarding the term-structure behaviour) suggests a consistently negative correlation between the expansions $\Sigma^{(0,0)}$ and $\Sigma^{(0,0)}_{1,0}$ of the model-version level and term-structure slope. According to the closed-form formulae of $\Sigma^{(0,0)}$ and $\Sigma^{(0,0)}_{1,0}$, all the models listed in Panel A of Table 3 are capable of generating such a negative correlation under some suitable conditions on the model parameters. Take the Heston and the GARCH-SV model as two illustrative examples. According to Table 6, under both of the two models, the level $\Sigma^{(0,0)}$ is equal to the spot volatility $\sqrt{v}$. Besides, applying our general result of the IV sensitivity expansion given in Theorem S.1, the expansion $\Sigma^{(0,0)}_{1,0}$ is given by

$$\Sigma^{(0,0)}_{1,0}(\tau, 0, v) = \frac{1}{96\sqrt{v}}[24\kappa\theta + \xi(24\rho(d-r) + \xi(\rho^2 - 4))] + \frac{\sqrt{v}}{8}(\xi\rho - 2\kappa), \tag{50}$$

for the Heston model, and

$$\Sigma^{(0,0)}_{1,0}(\tau, 0, v) = \frac{\xi\rho}{4}(d-r) + \frac{\theta\kappa}{4\sqrt{v}} + \frac{\xi\rho v}{8} - \frac{\sqrt{v}}{96}(24\kappa + \xi^2(3\rho^2 + 4)),$$

for the GARCH-SV model, respectively. Thus, as the level $\Sigma^{(0,0)}(\tau, 0, v) = \sqrt{v}$ increases, the term-structure slope $\Sigma^{(0,0)}_{1,0}$ decreases under the Heston (resp. GARCH-SV) model, if $24\rho(d-r) + \xi(\rho^2 - 4) > 0$ and $\rho < 0$ (resp. $\rho < 0$).

In regard to *Stylized fact 4*, none of the continuous one-factor SV models listed in Panel A of Table 3 are capable of producing a positively explosive convexity as the time-to-maturity shrinks to zero. Indeed, by computation, the leading term $\sigma^{(-1,0)}_{0,2}(x)$ of the zeroth order convexity expansion (47) is calculated as zero for any continuous SV model. Owing to the absence of negative powers of ϵ, it follows from expansion (47) that the at-the-money convexity converges to $\sigma^{(0,0)}_{0,2}(x)$, which is a finite value, as the time-to-maturity shrinks to zero. This nonexplosive nature of continuous models restricts their potential application to some time periods, in which most of the short-maturity convexities are negatively finite, e.g., the period of October 5, 2016 to October 18, 2016 as shown in the right panel of Fig. 6.

We can additionally use the shape characteristics formulae to obtain bounds for the model parameters. Take the Heston model as an illustration: According to the box plots in Fig. 5, the means of level, slope, and convexity for time-to-maturity equal to 30 days are approximately 0.13, -0.9, and 3.8, respectively. By matching these three shape characteristics with the corresponding closed-form formulae of level $\Sigma^{(0,0)}$, slope $\Sigma^{(0,0)}_{0,1}$, and convexity $\Sigma^{(0,0)}_{0,2}$ given in Table 6, the volatility-of-variance parameter ξ is obtained as 0.8, which is higher than the usual values estimated in the literature from the time series dynamics of underlying asset. Given a typical estimated value of the long-run mean of variance θ, e.g., 0.04 (corresponding to 20% annualized volatility), Feller's condition $\kappa \geq \xi^2/(2\theta)$ forces the speed of mean-reversion parameter κ to be at least 8, which is also higher than most of the existing estimators in the literature. The conclusion is that the

Heston model is not capable of fitting the shape characteristics of the IV surface. Alternatively, one can regard the lower bound of κ implied by the IV shape characteristics as an additional constraint to be added to existing estimation methods.

To summarize, the analysis so far reveals the merits of one-factor models in partially explaining the four stylized facts and two potential limitations, i.e., the lack of flexibility in reproducing enough variation of the data of level and slope as well as the incapability of generating explosive at-the-money convexity as the time-to-maturity shrinks to zero. From the middle panel of Fig. 5, one may alternatively regard the at-the-money slope to be diverging to $-\infty$ (see discussions in, e.g., Fouque et al., 2004) as time-to-maturity approaching to zero. To explain such a pattern, alternative models, e.g., the rough volatility model in Bayer et al. (2016) or the Levy-driven model in Figueroa-López and Ólafsson (2016) need to be considered. However, extrapolation in time-to-maturity can be problematic since options with extremely short maturities are noisy. We find that the mean tends to decrease, as the time-to-maturity decreases. But there is no strong evidence of slope diverging to $-\infty$.

5.2. The benefits of adding a second SV factor

Can we do better by adding a second SV state variable? A variety of existing two-factor continuous SV models are listed in Panel B of Table 3. For the DMR-SQR model, we obtain that the expansions $\Sigma^{(0,0)}$, $\Sigma^{(0,0)}_{0,1}$, and $\Sigma^{(0,0)}_{0,2}$ for level, slope, and convexity, respectively, are identical to those under the Heston model, as shown in Table 6. Hence, the correlation between level and slope under the DMR-SQR model is restricted to be positive, for the same reason as under the Heston model. Moreover, since the expansions $\Sigma^{(0,0)}$ and $\Sigma^{(0,0)}_{0,1}$ are determined only by the first volatility factor V_t, it is impossible for the DMR-SQR model to outperform the Heston model in terms of reproducing the variation of the data of level and slope.

Besides the coincidence of level, slope, and convexity, the term-structure slope expansion $\Sigma^{(0,0)}_{1,0}$ under the DMR-SQR model is similar to that under the Heston model except for replacing the long-run mean θ in (50) by the added volatility factor $\bar{v}$, i.e.,

$$\Sigma^{(0,0)}_{1,0}(\tau, 0, v, \bar{v}) = \frac{1}{96\sqrt{v}}[24\kappa\bar{v} + \xi(24\rho(d-r) + \xi(\rho^2 - 4))] + \frac{\sqrt{v}}{8}(\xi\rho - 2\kappa).$$

So the dynamics of term-structure slope under the DMR-SQR model permits more flexibility, because it is driven by two SV factors V_t and $\bar{V}_t$, in contrast to a single factor V_t under the Heston model.[15]

To relax these limitations of the square root specification, generalizations ought to be performed on the diffusion component of the SV model. The double-SQR model proposed by Christoffersen et al. (2009) modifies the Heston model by adding another SV factor to the diffusion. This generalization has three advantages. First, the correlation between level and slope is not necessarily to be positive: for example, uncorrelated level and slope can be generated as long as

$$\text{Corr}(\Sigma^{(0,0)}, \Sigma^{(0,0)}_{0,1}) = \text{Corr}\left(\sqrt{V_{1t} + V_{2t}}, \frac{\xi_1\rho_1 V_{1t} + \xi_2\rho_2 V_{2t}}{4(V_{1t} + V_{2t})^{3/2}}\right) = 0,$$

which on the other hand requires a rather specific nonlinear constraint of the parameters. As opposed to the one-factor log-OU and GARCH-SV model discussed in Section 5.1, the double-SQR model provides no correlation without imposing that the slope expansion $\Sigma^{(0,0)}_{0,1}$ is constant. Second, even for a fixed level expansion $\Sigma^{(0,0)}(\tau, 0, v_1, v_2) = \sqrt{v_1 + v_2}$, the slope expansion

$$\Sigma^{(0,0)}_{0,1}(\tau, 0, v_1, v_2) = \frac{1}{4}(v_1\xi_1\rho_1 + v_2\xi_2\rho_2)(v_1 + v_2)^{-\frac{3}{2}}$$

varies, owing to different combinations of v_1 and v_2. So the double-SQR model is better able to capture the variation of the data exhibited in Fig. 2. Third, similar to the above discussion on the dynamics of term-structure slope under the DMR-SQR model, the dynamics of level, slope, and convexity under the double-SQR model permit more flexibility. This is because these shape characteristics are driven by two SV factors V_{1t} and V_{2t}. The double-log-linear model shares with the double-SQR model all the aforementioned advantages; we omit a detailed discussion for this model.

Even though they are significantly more flexible than their corresponding one-factor counterparts, two-factor continuous SV models are still incapable of generating the explosive at-the-money convexities documented in *Stylized fact 4*. For this, jumps are needed.

5.3. The benefits of adding jumps in returns

As discussed in Section 4.2, any SV model with jumps is capable of generating an explosive at-the-money convexity towards the positive infinity as the time-to-maturity shrinks to zero. This fits what we observe in IV surfaces as *Stylized fact 4*. Furthermore, according to the convexity expansion (36), the rate of explosion with respect to the time-to-maturity τ is -0.5. On the other hand, for the subsample presented in the left panel of Fig. 6, the explosion is characterized by fitting the data with the nonlinear regression (1), i.e., $\text{convexity}_i = a\tau_i^b + c + \epsilon_i$. The coefficient b characterizes the rate of explosion. It is estimated as -0.45, which is indeed close to -0.5.

[15] The advantages of the DMR-SQR model over the Heston model in terms of modelling the term structure of variance swap rates can be found in, for example, Egloff et al. (2010) and Aït-Sahalia et al. (2019) among others.

Table 7
Closed-form formulae for at-the-money level, slope, and convexity expansions for the SV models with jumps listed in Table 4.

Model	Expansions of the model-version level, slope, and convexity		
	Level: $\Sigma^{(0,0)}$	Slope: $\Sigma^{(0,0)}_{0,1}$	Convexity: $\Sigma^{(0,0)}_{0,2}$
Panel A: One-factor SV models with jumps			
One-factor affine SV with jumps	$\sqrt{v}$	$[4(\lambda_0+\lambda_1 v)\bar{\mu}+\xi\rho]/(4\sqrt{v})$	$\sigma^{(-1,0)}_{0,2}=\sqrt{\pi}(\lambda_0+\lambda_1 v)(-\bar{\mu}+2(\bar{\mu}+1)\mathcal{N}(\mu_+)-2\mathcal{N}(\mu_-))/(\sqrt{2}v)$ $\sigma^{(0,0)}_{0,2}=[2(\xi^2-6(\lambda_0+\lambda_1 v)(2\bar{\mu}(-2d+2r+v)+\pi\bar{\mu}^2(\lambda_0+\lambda_1 v)+4v))$ $-5\xi^2\rho^2-12\bar{\mu}\xi\rho(\lambda_0+\lambda_1 v)+48\pi(\lambda_0+\lambda_1 v)^2(-(\bar{\mu}+1)^2\mathcal{N}(\mu_+)^2$ $-\mathcal{N}(\mu_-)(\bar{\mu}+\mathcal{N}(\mu_-))+(\bar{\mu}+1)\mathcal{N}(\mu_+)(\bar{\mu}+2\mathcal{N}(\mu_-)))]/(24v^{3/2})$
Log-OU SV with jumps	e^u	$(\lambda_0 e^{-u}+\lambda_1 e^u)\bar{\mu}+\xi\rho/2$	$\sigma^{(-1,0)}_{0,2}=\sqrt{\pi/2}(\lambda_0 e^{-2u}+\lambda_1)(-\bar{\mu}+2(\bar{\mu}+1)\mathcal{N}(\mu_+)-2\mathcal{N}(\mu_-))$ $\sigma^{(0,0)}_{0,2}=[6(\lambda_0+\lambda_1 e^{2u})\left(2\bar{\mu}(d-r)-\bar{\mu}\xi\rho e^u-(\bar{\mu}+2)e^{2u}\right)+\xi^2(2-3\rho^2)e^{2u}$ $-3\pi(\lambda_0+\lambda_1 e^{2u})^2(\bar{\mu}-2(\bar{\mu}+1)\mathcal{N}(\mu_+)+2\mathcal{N}(\mu_-))^2]/(6e^{3u})$
Panel B: Two-factor SV models with jumps			
Two-factor affine SV with jumps	$\sqrt{v_1+v_2}$	$(\xi_1\rho_1 v_1+\xi_2\rho_2 v_2)/(4(v_1+v_2)^{3/2})+\bar{\mu}(\lambda_0+\lambda_1 v_1+\lambda_2 v_2)/\sqrt{v_1+v_2}$	$\sigma^{(-1,0)}_{0,2}=\sqrt{\pi/2}(\lambda_0+\lambda_1 v_1+\lambda_2 v_2)(-\bar{\mu}+2(\bar{\mu}+1)\mathcal{N}(\mu_+)-2\mathcal{N}(\mu_-))/(v_1+v_2)$ $\sigma^{(0,0)}_{0,2}=[-12v_1^3(2\bar{\mu}(\lambda_0+2\lambda_1(r-d)+(3\lambda_1+\lambda_2)v_2)+2\pi\lambda_1\bar{\mu}^2(\lambda_0+(\lambda_1+\lambda_2)v_2)$ $+\lambda_1\bar{\mu}\xi_1\rho_1+4(\lambda_0+(3\lambda_1+\lambda_2)v_2))-v_1^2(12\lambda_0\bar{\mu}(\pi\lambda_0\bar{\mu}+4(r-d))-2\xi_1^2$ $+12v_2(\bar{\mu}(4(r-d)(2\lambda_1+\lambda_2)+\xi_1\rho_1(\lambda_1+\lambda_2)+\lambda_1\xi_2\rho_2)$ $+2\lambda_0(\bar{\mu}(\pi\bar{\mu}(2\lambda_1+\lambda_2)+3)+6))+12\lambda_0\bar{\mu}\xi_1\rho_1+12v_2^2(\pi\bar{\mu}^2(\lambda_1^2+4\lambda_1\lambda_2+\lambda_2^2)$ $+6\bar{\mu}(\lambda_1+\lambda_2)+12(\lambda_1+\lambda_2))+5\xi_1^2\rho_1^2)-2v_1v_2(12(\lambda_0\bar{\mu}(\pi\lambda_0\bar{\mu}+4(r-d))$ $-2v_2\bar{\mu}(d-r)(\lambda_1+2\lambda_2)+v_2^2\left(\pi\lambda_2\bar{\mu}^2(\lambda_1+\lambda_2)+\bar{\mu}(\lambda_1+3\lambda_2)+2\lambda_1+6\lambda_2\right)$ $+v_2(\lambda_0(\bar{\mu}(\pi\bar{\mu}(\lambda_1+2\lambda_2)+3)+6)))+3\xi_2\rho_2(3\xi_1\rho_1+2\bar{\mu}(\lambda_0+v_2(\lambda_1+\lambda_2)))$ $-2\xi_1^2\rho_1^2-\xi_1^2-2\xi_2^2\rho_2^2-\xi_2^2+6\bar{\mu}\xi_1\rho_1(\lambda_0+\lambda_2 v_2))-v_2^2(12\bar{\mu}\xi_2\rho_2(\lambda_0+\lambda_2 v_2)$ $+12(\lambda_0+\lambda_2 v_2)\left(2\bar{\mu}(2(r-d)+v_2)+\pi\bar{\mu}^2(\lambda_0+\lambda_2 v_2)+4v_2\right)+5\xi_2^2\rho_2^2-2\xi_2^2)$ $-12\lambda_1 v_1^4(\mu(\pi\lambda_1\bar{\mu}+2)+4)-48\pi(v_1+v_2)^2(-\bar{\mu}+(\bar{\mu}+1)\mathcal{N}(\mu_+)-\mathcal{N}(\mu_-))$ $\times((\bar{\mu}+1)\mathcal{N}(\mu_+)-\mathcal{N}(\mu_-))(\lambda_0+\lambda_1 v_1+\lambda_2 v_2)^2]/24(v_1+v_2)^{7/2}$
DMR-SQR SV with jumps	$\sqrt{v}$	$[4(\lambda_0+\lambda_1 v)\bar{\mu}+\xi\rho]/(4\sqrt{v})$	$\sigma^{(-1,0)}_{0,2}=\sqrt{\pi}(\lambda_0+\lambda_1 v)(-\bar{\mu}+2(\bar{\mu}+1)\mathcal{N}(\mu_+)-2\mathcal{N}(\mu_-))/(\sqrt{2}v)$ $\sigma^{(0,0)}_{0,2}=[2(\xi^2-6(\lambda_0+\lambda_1 v)(2\bar{\mu}(-2d+2r+v)+\pi\bar{\mu}^2(\lambda_0+\lambda_1 v)+4v))$ $-5\xi^2\rho^2-12\bar{\mu}\xi\rho(\lambda_0+\lambda_1 v)+48\pi(\lambda_0+\lambda_1 v)^2(-(\bar{\mu}+1)^2\mathcal{N}(\mu_+)^2$ $-\mathcal{N}(\mu_-)(\bar{\mu}+\mathcal{N}(\mu_-))+(\bar{\mu}+1)\mathcal{N}(\mu_+)(\bar{\mu}+2\mathcal{N}(\mu_-)))]/(24v^{3/2})$

For discovering more benefits of including jumps, we now compare the one-factor affine SV model with jumps (resp. the log-OU SV model with jumps) listed in Panel A of Table 4 with the Heston model (resp. the log-OU model) listed in Panel A of Table 3. Table 7 reports the closed-form expansions of level $\Sigma^{(0,0)}$, slope $\Sigma^{(0,0)}_{0,1}$, and convexity $\Sigma^{(0,0)}_{0,2}$ calculated by applying our general expansion results of the IV and its sensitivities given in Theorem S.1, under all four SV models with jumps listed in Table 4.

Under the one-factor affine SV model with jumps, the slope expansion $\Sigma^{(0,0)}_{0,1}$ is given by

$$\Sigma^{(0,0)}_{0,1}(\tau,0,v)=\frac{\xi\rho}{4\sqrt{v}}+\frac{1}{\sqrt{v}}(\lambda_0+\lambda_1 v)\bar{\mu},$$

as documented in the first row of Panel A in Table 7, where $\bar{\mu}$ is the mean jump size defined in (3), i.e., $\bar{\mu}=\mathbb{E}[\exp(J_t)]-1$. Unlike what happens under the Heston model, the presence of stochastic intensity and asymmetric jumps, i.e., $\lambda_1\neq 0$ and $\bar{\mu}\neq 0$, enables a one-factor affine SV model with jumps to produce a non-monotonic relation between the level ($\Sigma^{(0,0)}$) and slope ($\Sigma^{(0,0)}_{0,1}$) expansions. For instance, given a negative leverage effect parameter ρ and a negative mean of jumps $\bar{\mu}$, the slope increases (resp. decreases), as the level $\Sigma^{(0,0)}(\tau,0,v)=\sqrt{v}$ increases, if v is less (resp. greater) than $(\xi\rho+4\lambda_0\bar{\mu})/(4\lambda_1\bar{\mu})$.

As for the log-OU SV model with jumps, the presence of asymmetric jumps leads to the fact that the slope expansion $\Sigma^{(0,0)}_{0,1}$ is state-dependent and thus stochastic, as opposed to being constant under the log-OU model without jumps. This can be seen in the slope expansion $\Sigma^{(0,0)}_{0,1}$ given in the second row of Panel A from Table 7, i.e.,

$$\Sigma^{(0,0)}_{0,1}(\tau,0,u)=(\lambda_0 e^{-u}+\lambda_1 e^u)\bar{\mu}+\frac{\xi\rho}{2}.$$

In particular, by setting the mean $\bar{\mu}$ to be zero, i.e., assuming jumps to be symmetric, the slope $\Sigma^{(0,0)}_{0,1}$ degenerates to a constant $\xi\rho/2$ independent of any jump parameters. In this case, even if a jump term exists in the SV model and generates impact on the IV convexity and term-structure slope, the IV level and slope become trivially uncorrelated, as in the corresponding continuous case, i.e., the log-OU model without jumps.

6. Conclusions and future directions

We develop in this paper a closed-form expansion for the shape characteristics of the IV surface, with respect to time-to-maturity and log-moneyness, when the model is a generic SV model with possibly jumps in returns. The formulae

provide an explicit link between the model and the data. In particular, it makes possible the analysis of the impact of specific parameters of a given SV model on the resulting IV surface. These explicit formulae explain the short-maturity behaviour of the IV shape characteristics and reveal a host of parameter impacts that were previously unknown. Using the formulae, we find that one-factor continuous SV models have limitations in fitting the four documented stylized facts of the IV data. Adding a second SV state variable helps match some of the stylized facts, such as those regarding the slope of moneyness dimension and/or the slope of the IV term structure. Finally, the presence of jumps widens the possible dependence between IV level and log-moneyness slope, and allows the model to generate positively explosive convexity in the log-moneyness dimension, as the time-to-maturity shrinks to zero.

Appendix A. Supplementary data

Supplementary material related to this article can be found online at https://doi.org/10.1016/j.jeconom.2020.07.006.

References

Aït-Sahalia, Y., Amengual, D., Manresa, E., 2015. Market-based estimation of stochastic volatility models. J. Econometrics 187, 418–435.
Aït-Sahalia, Y., Karaman, M., Mancini, L., 2019. The term structure of equity and variance risk premia. J. Econometrics forthcoming.
Aït-Sahalia, Y., Kimmel, R., 2007. Maximum likelihood estimation of stochastic volatility models. J. Financ. Econ. 83, 413–452.
Aït-Sahalia, Y., Li, C., Li, C.X., 2020. Implied stochastic Volatility models. Rev. Financ. Stud. forthcoming.
Aït-Sahalia, Y., Lo, A., 1998. Nonparametric estimation of state-price-densities implicit in financial asset prices. J. Finance 53, 499–547.
Andersen, T.G., Benzoni, L., Lund, J., 2002. An empirical investigation of continuous-time equity return models. J. Finance 57, 1239–1284.
Andersen, T.G., Fusari, N., Todorov, V., 2015. The risk premia embedded in index options. J. Financ. Econ. 117, 558–584.
Andersen, L., Lipton, A., 2013. Asymptotics for exponential Lévy processes and their volatility smile: Survey and new results. Int. J. Theor. Appl. Finance 16, 1–98.
Bakshi, G., Cao, C., Chen, Z., 1997. Empirical performance of alternative option pricing models. J. Finance 52, 2003–2049.
Bardgett, C., Gourier, E., Leippold, M., 2019. Inferring volatility dynamics and risk-premia from the S & P 500 and VIX markets. J. Financ. Econ. 131, 593–618.
Bates, D.S., 1996. Jumps and stochastic volatility: Exchange rate processes implicit in Deutsche Mark options. Rev. Financ. Stud. 9, 69–107.
Bates, D.S., 2000. Post-'87 crash fears in the S & P 500 futures option market. J. Econometrics 94, 181–238.
Bayer, C., Friz, P., Gatheral, J., 2016. Pricing under rough volatility. Quant. Finance 16, 887–904.
Benhamou, E., Gobet, E., Miri, M., 2010. Time dependent Heston model. SIAM J. Financial Math. 1, 289–325.
Berestycki, H., Busca, J., Florent, I., 2004. Computing the implied volatility in stochastic volatility models. Comm. Pure Appl. Math. 57, 1352–1373.
Carr, P., Wu, L., 2003. The finite moment log stable process and option pricing. J. Finance 58, 753–777.
Carr, P., Wu, L., 2016. Analyzing volatility risk and risk premium in option contracts: A new theory. J. Financ. Econ. 120, 1–20.
Chernov, M., Gallant, A.R., Ghysels, E., Tauchen, G.T., 2003. Alternative models for stock price dynamics. J. Econometrics 116, 225–257.
Christoffersen, P., Heston, S., Jacobs, K., 2009. The shape and term structure of the index option smirk: Why multifactor stochastic volatility models work so well. Manage. Sci. 55, 1914–1932.
Christoffersen, P., Jacobs, K., Mimouni, K., 2010. Volatility dynamics for the S & P500: Evidence from realized volatility, daily returns, and option prices. Rev. Financ. Stud. 23 (8), 3141–3189.
Cont, R., da Fonseca, J., 2002. Dynamics of implied volatility surfaces. Quant. Finance 2, 45–60.
Cox, J.C., 1975. The constant elasticity of variance option pricing model. J. Portfolio Manag. 22, 15–17 (1996 special issue).
Duffie, D., Pan, J., Singleton, K.J., 2000. Transform analysis and asset pricing for affine jump-diffusions. Econometrica 68, 1343–1376.
Dupire, B., 1994. Pricing with a smile. RISK 7, 18–20.
Durrleman, V., 2008. Convergence of at-the-money implied volatilities to the spot volatility. J. Appl. Probab. 45, 542–550.
Durrleman, V., 2010. From implied to spot volatilities. Finance Stoch. 14 (2), 157–177.
Egloff, D., Leippold, M., Wu, L., 2010. The term structure of variance swap rates and optimal variance swap investments. J. Financ. Quant. Anal. 45, 1279–1310.
Eraker, B., Johannes, M.S., Polson, N., 2003. The impact of jumps in equity index volatility and returns. J. Finance 58, 1269–1300.
Figueroa-López, J.E., Ólafsson, S., 2016. Short-term asymptotics for the implied volatility skew under a stochastic volatility model with Lévy jumps. Finance Stoch. 20, 973–1020.
Forde, M., Jacquier, A., Lee, R., 2012. The small-time smile and term structure of implied volatility under the Heston model. SIAM J. Financial Math. 3 (1), 690–708.
Fouque, J.-P., Lorig, M., Sircar, R., 2016. Second order multiscale stochastic volatility asymptotics: Stochastic terminal layer analysis and calibration. Finance Stoch. 63, 1648–1665.
Fouque, J.-P., Papanicolaou, G., Sircar, R., Solna, K., 2003. Multiscale stochastic volatility asymptotics. Multiscale Model. Simul. 2, 22–42.
Fouque, J.-P., Papanicolaou, G., Sircar, R., Solna, K., 2004. Maturity cycles in implied volatility. Finance Stoch. 8, 451–477.
Fukasawa, M., 2011a. Asymptotic analysis for stochastic volatility: Edgeworth expansion. Electron. J. Probab. 16, 764–791.
Fukasawa, M., 2011b. Asymptotic analysis for stochastic volatility: Martingale expansion. Finance Stoch. 15, 635–654.
Fukasawa, M., 2017. Short-time at-the-money skew and rough fractional volatility. Quant. Finance 17, 189–198.
Gallant, A.R., Hsu, C.-T., Tauchen, G.T., 1999. Using daily range data to calibrate volatility diffusions and extract the forward integrated variance. Rev. Econ. Stat. 81, 617–631.
Gao, K., Lee, R., 2014. Asymptotics of implied volatility to arbitrary order. Finance Stoch. 18 (2), 349–392.
Gatheral, J., 2006. The Volatility Surface: A Pactitioner's Guide. John Wiley and Sons, Hoboken, NJ.
Gatheral, J., Hsu, E.P., Laurence, P., Ouyang, C., Wang, T.-H., 2012. Asymptotics of implied volatility in local volatility models. Math. Finance 22 (4), 591–620.
Hagan, P.S., Woodward, D.E., 1999. Equivalent Black volatilities. Appl. Math. Finance 6, 147–157.
Henry-Labordère, P., 2008. Analysis, Geometry, and Modeling in Finance: Advanced Methods in Option Pricing. CRC Press, Boca Raton, FL.
Heston, S., 1993. A closed-form solution for options with stochastic volatility with applications to bonds and currency options. Rev. Financ. Stud. 6, 327–343.
Hull, J., White, A., 1987. The pricing of options on assets with stochastic volatilities. J. Finance 42, 281–300.
Jones, C.S., 2003. The dynamics of stochastic volatility: Evidence from underlying and options markets. J. Econometrics 116, 181–224.
Krantz, S., Parks, H., 2003. The Implicit Function Theorem, first ed. Birkhäuser, Boston.

Kristensen, D., Mele, A., 2011. Adding and subtracting Black-Scholes: A new approach to approximating derivative prices in continuous-time models. J. Financ. Econ. 102, 390–415.
Kunitomo, N., Takahashi, A., 2001. The asymptotic expansion approach to the valuation of interest rate contingent claims. Math. Finance 11, 117–151.
Ledoit, O., Santa-Clara, P., Yan, S., 2002. Relative Pricing of Options with Stochastic Volatility. Tech. rep., University of California, Los Angeles.
Lorig, M., Pagliarani, S., Pascucci, A., 2017. Explicit implied volatilities for multifactor local-stochastic volatility models. Math. Finance 27, 927–960.
Meddahi, N., 2001. An Eigenfunction Approach for Volatility Modeling. Tech. rep., Université de Montréal.
Medvedev, A., Scaillet, O., 2007. Approximation and calibration of short-term implied volatilities under jump-diffusion stochastic volatility. Rev. Financ. Stud. 20, 427–459.
Merton, R.C., 1976. Option pricing when underlying stock returns are discontinuous. J. Financ. Econ. 3, 125–144.
Mixon, S., 2009. Option markets and implied volatility: Past versus present. J. Financ. Econ. 94, 171–191.
Nelson, D.B., 1990. ARCH models as diffusion approximations. J. Econometrics 45, 7–38.
Pan, J., 2002. The jump-risk premia implicit in options: Evidence from an integrated time-series study. J. Financ. Econ. 63, 3–50.
Schöbel, R., Zhu, J., 1999. Stochastic volatility with an Ornstein-Uhlenbeck process: An extension. Eur. Finance Rev. 3 (1), 23–46.
Schönbucher, P.J., 1999. A market model for stochastic implied volatility. Philos. Trans. R. Soc. Lond. Ser. A 357, 2071–2092.
Scott, L.O., 1987. Option pricing when the variance changes randomly: Theory, estimation, and an application. J. Financ. Quant. Anal. 22, 419–438.
Stein, E.M., Stein, J.C., 1991. Stock price distributions with stochastic volatility: An analytic approach. Rev. Financ. Stud. 4, 727–752.
Takahashi, A., Yamada, T., 2012. An asymptotic expansion with push-down of Malliavin weights. SIAM J. Financial Math. 3, 95–136.
Todorov, V., 2019. Nonparametric spot volatility from options. Ann. Appl. Probab. 29 (6), 3590–3636.
Xiu, D., 2014. Hermite polynomial based expansion of European option prices. J. Econometrics 179, 158–177.
Yan, S., 2011. Jump risk, stock returns, and slope of implied volatility smile. J. Financ. Econ. 99 (1), 216–233.